The Journal of Physiology

Role of forelimb morphology in muscle sensorimotor functions during locomotion in the cat

Seyed Mohammadali Rahmati[1], Alexander N. Klishko[1], Ramaldo S. Martin[2], Nate E. Bunderson[3], Jeswin A. Meslie[1], T. Richard Nichols[1], Ilya A. Rybak[4], Alain Frigon[5], Thomas J. Burkholder[1] and Boris I. Prilutsky[1]

[1]*School of Biological Sciences, Georgia Institute of Technology, Atlanta, GA, USA*
[2]*AVEVA, San Leandro, CA, USA*
[3]*Autonomous Solutions, Petersboro, UT, USA*
[4]*Department of Neurobiology and Anatomy, Drexel University, Philadelphia, PA, USA*
[5]*Department of Pharmacology-Physiology, Université de Sherbrooke, Sherbrooke, Quebec, Canada*

Handling Editors: Richard Carson & Vaughan Macefield

The peer review history is available in the Supporting Information section of this article (https://doi.org/10.1113/JP287448#support-information-section).

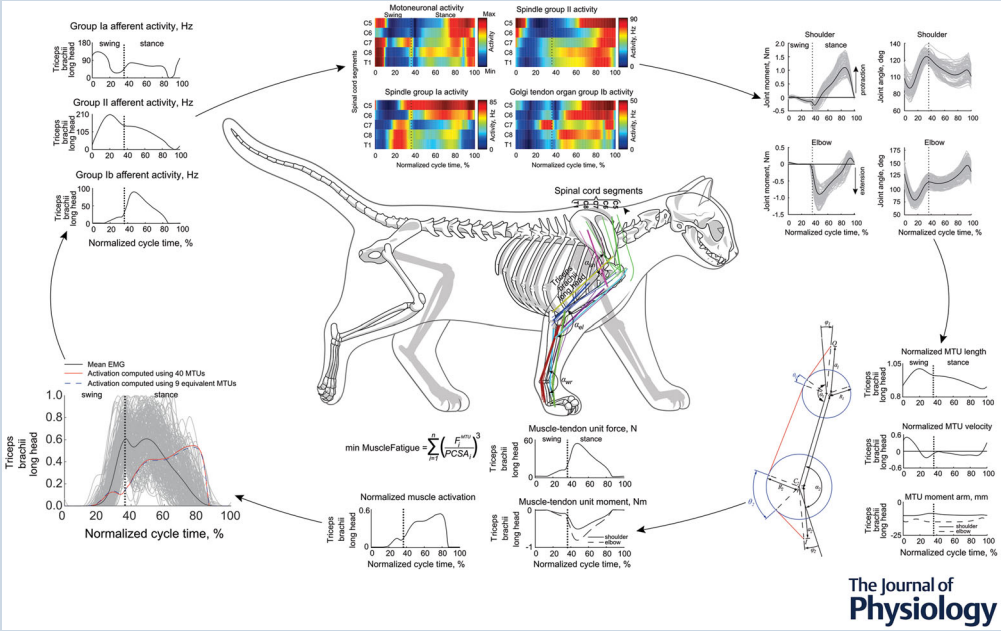

Abstract figure legend Experimentally obtained and computed neuromechanical variables characterizing sensorimotor functions of cat forelimb muscles during locomotion.

T. J. Burkholder and B. I. Prilutsky contributed equally to this work.

This article was first published as a preprint. Rahmati SM, Klishko AN, Martin RS, Bunderson NE, Meslie JA, Nichols TR, Rybak IA, Frigon A, Burkholder TJ, Prilutsky BI. 2024. Role of forelimb morphology in muscle sensorimotor functions during locomotion in the cat. bioRxiv. https://doi.org/10.1101/2024.07.11.603106

DOI: 10.1113/JP287448

Abstract Previous studies established strong links between morphological characteristics of mammalian hindlimb muscles and their sensorimotor functions during locomotion. Less is known about the role of forelimb morphology in motor outputs and generation of sensory signals. Here, we measured morphological characteristics of 46 forelimb muscles from six cats. These characteristics included muscle attachments, physiological cross-sectional area (PCSA) and fascicle length. We also recorded full-body mechanics and EMG activity of forelimb muscles during level overground and treadmill locomotion in seven and 16 adult cats of either sex, respectively. We computed forelimb muscle forces along with force- and length-dependent sensory signals mapped onto corresponding cervical spinal segments. We found that patterns of computed muscle forces and afferent activities were strongly affected by the muscle's moment arm, PCSA and fascicle length. Morphology of the shoulder muscles suggests distinct roles of the forelimbs in lateral force production and movements. Patterns of length-dependent sensory activity of muscles with long fibres (brachioradialis, extensor carpi radialis) closely matched patterns of overall forelimb length, whereas the activity pattern of biceps brachii length afferents matched forelimb orientation. We conclude that cat forelimb muscle morphology contributes substantially to locomotor function, particularly to control lateral stability and turning, rather than propulsion.

(Received 5 August 2024; accepted after revision 19 November 2024; first published online 19 December 2024)
Corresponding author B. I. Prilutsky: School of Biological Sciences, Georgia Institute of Technology, 555 14th Street NW, Atlanta, GA 30332-0356, USA. Email: boris.prilutsky@ap.gatech.edu

Key points

- Little is known about the role of forelimb muscle morphology in producing motor outputs and generating somatosensory signals. This information is needed to understand the contributions of forelimbs in locomotor control.
- We measured morphological characteristics of 46 muscles from cat forelimbs, recorded cat walking mechanics and electromyographic activity, and computed patterns of moment arms, length, velocity, activation, and force of forelimb muscles, as well as length- and force-dependent afferent activity during walking.
- We demonstrated that moment arms, physiological cross-sectional area and fascicle length of forelimb muscles contribute substantially to muscle force production and proprioceptive activity, to the regulation of locomotor cycle phase transitions and to control of lateral stability.
- The obtained information can guide the development of biologically accurate neuromechanical models of quadrupedal locomotion for exploring and testing novel methods of treatments of central nervous system pathologies by modulating activities in neural pathways controlling forelimbs/arms.

Introduction

Quadrupedal mammals evolved their musculoskeletal and neural sensorimotor systems to perform various locomotor behaviours, such as searching for food, escaping predators and finding mates to produce offspring. Evolutionary history and functional demands are critical factors defining the morphology of animal

Seyed Mohammadali Rahmati holds a PhD in Biomedical Engineering from Amirkabir University of Technology, Iran. As a Postdoctoral Fellow at Georgia Tech, he conducts research in experimental and computational neuromechanics and sensorimotor control of locomotion. He has investigated feline forelimb neuromechanics during locomotion. Separately, he has worked on reconstructing rat 3D skeletal locomotor kinematics from biplanar X-ray video recordings using deep learning and singular value decomposition. He also contributed to projects investigating the role of proprioception in locomotor stability in mice and optimal muscle activation strategies in cats. His work aims to advance the understanding of movement science through neuromechanics.

limbs and their sensorimotor functions (Diogo & Molnar, 2014; Rothier et al., 2023; Shubin et al., 1997). Mammalian forelimbs and hindlimbs have evolved many common morphological features. For instance, three-segment kinematic chains (i.e. upper arm–forearm–metacarpus and thigh–shank–metatarsus) are designed to save energy and improve stability (Fischer & Blickhan, 2006; Kuznetsov, 1995). A distal-to-proximal gradient of limb inertia with larger muscles located around proximal joints allows for faster and more economical swing and reaching movements (Charles, Cappellari, Spence, Hutchinson et al., 2016; Gambaryan, 1974; Hudson et al., 2011a,b; Kilbourne & Carrier, 2016; Martin et al., 2010; Mathewson et al., 2012) and paw shake responses (Prilutsky et al., 2022). A significant redundancy of muscle action, with over 30 muscles serving just seven major degrees of freedom (Bunderson et al., 2010; Burkholder & Nichols, 2004; Martin et al., 2010; Prilutsky & Zatsiorsky, 2002; Ramalingasetty et al., 2021; Stark et al., 2021) is only partially resolved by considering non-sagittal actions. The presence of two-joint muscles in the hindlimb and forelimb contributes to regulating limb stiffness and impedance, inter-joint coordination, reducing exergy expenditure and muscle fatigue, and distribution of mechanical energy along the limb (Elftman, 1940; Nichols, 1994; Prilutsky, 2000a,b; Van Ingen Schenau et al., 1994). Similarities in limb morphology between the fore- and hindlimb correspond to a generally similar organization of excitatory and inhibitory somatosensory pathways. For example, the monosynaptic excitatory and bi-synaptic inhibitory Ia muscle length-dependent pathways in the cat hindlimb (Eccles & Lundberg, 1958; Eccles et al., 1957a; Edgley et al., 1986; Nichols, 1994, 1999) and forelimb (Caicoya et al., 1999; Fritz et al., 1989; Illert, 1996), along with Ib pathways (Eccles et al., 1957b; Nichols, 2018) and recurrent inhibition pathways (Eccles et al., 1961; Illert & Wietelmann, 1989; Turkin et al., 1998) coordinate synergistic activities of agonists and antagonists at and across joints, although these pathways appear more complex in the forelimb (Fritz et al., 1989). The greater volume (the product of the mean physiological cross-sectional area [PCSA] and muscle fascicle length) of proximal *vs*. distal muscles in the forelimbs and hindlimbs typically results in longer muscle moment arms of proximal muscles (Burkholder & Nichols, 2004; Charles, Cappellari, Spence, Wells et al., 2016; Graham & Scott, 2003; Hudson et al., 2011a,b; Ramalingasetty et al., 2021). This translates into a higher acuity of length-dependent afferents to angle changes in proximal joints compared to distal ones (Burkholder & Nichols, 2000; Hall & McCloskey, 1983; Oh & Prilutsky, 2022). This feature of hip muscles could explain their important role in triggering the stance–swing (Kriellaars et al., 1994; Lam & Pearson, 2001) and swing–stance (Gregor et al., 2006; McVea et al., 2005) transitions during cat locomotion.

There are also differences in morphology and function between the forelimbs and hindlimbs. One of the most noticeable is the opposite flexion–extension directions in the homologous elbow and knee joints, which is likely caused by a much broader functional repertoire of the forelimbs, with unique roles in exploratory, hunting, reaching and grasping behaviours. The mass and volume of hindlimb muscles are greater than those of the forelimbs (Gambaryan, 1974; Hudson et al., 2011a,b; Ramalingasetty et al., 2021), although the forelimbs support a greater fraction of body weight than the hindlimbs due to a more rostral position of the body's centre of mass (Frigon et al., 2022; Grey, 1944). Larger muscle volume in the hindlimbs permits greater production of positive power/work and body acceleration compared to the forelimbs during locomotion (Dutto et al., 2006; Gregersen et al., 1998; Jarrell et al., 2018; Pandy et al., 1988). The forelimbs contribute more to body deceleration and the absorption of body energy (the production of negative power/work) than the hindlimbs during locomotion with constant speeds (Corbee et al., 2014; Dutto et al., 2004; Dutto et al., 2006; Farrell et al., 2014). It is expected that differences in morphology and mechanical functions between mammalian hindlimbs and forelimbs are also reflected in differences in their neural control.

Knowledge of limb morphology and its roles in sensorimotor functions is critically important for understanding the neural control of quadrupedal locomotion because the nervous system evolved in parallel with the musculoskeletal system, integrating feedforward central mechanisms in the brain and spinal cord with motion-dependent somatosensory feedback (Arber & Costa, 2022; Danner et al., 2017; Dougherty, 2023; Frigon et al., 2022; Grillner & El Manira, 2020; Leiras et al., 2022; Yakovenko & Drew, 2015). Previous studies established strong links between morphological characteristics of hindlimb muscles and their motor and sensory locomotor functions, especially in the cat (Bunderson et al., 2010; Burkholder & Lieber, 2001; Burkholder & Nichols, 2000; Charles, Cappellari, Spence, Hutchinson et al., 2016; Ekeberg & Pearson, 2005; He et al., 1991; Nichols, 1994; Prochazka, 1999; Spector et al., 1980; Yakovenko et al., 2002). However, little is known about the role of forelimb muscle morphology in producing motor outputs and generating length- and force-dependent sensory signals. This information is needed to understand the contributions of the forelimbs in controlling quadrupedal locomotion.

Therefore, the goal of this study was to determine the morphological characteristics of cat forelimb muscles and evaluate their contribution to locomotor kinetics and motion-dependent sensory feedback. We constructed a musculoskeletal model of the cat forelimb and validated select distal moment arms. We used kinematics and

kinetics collected from walking cats to estimate muscle activations during walking. We validated these predictions against selected EMG recordings. Finally, we estimated proprioceptive afferent activities and mapped them onto corresponding cervical spinal segments. This information provided unprecedented insight into the role of mammalian forelimb morphology in motor and somatosensory functions during locomotion.

Methods

Ethical approval

The experiments described in this study were in agreement with the US Public Health Service Policy on Humane Care and Use of Laboratory Animals and with the Canadian Council on Animal Care. All experimental procedures were reviewed and approved by the Institutional Animal Care and Use Committees of Georgia Institute of Technology (protocol number A13063) and Université de Sherbrooke (protocol number 442-18). The purpose-bred cats of either sex were purchased for this study from Liberty Research (Waverly, NY, USA) and Marshall BioResources (North Rose, NY, USA). Before and during the study, female and male cats were socially housed in two separate large rooms in the animal facility with access to food and water *ad libitum*. A day before training or data collection, one or two cats were placed overnight in a large two-level fasting cage with water and litter. The next morning, these cats were taken to the research laboratory for training or data collection for up to 5 h and received a full daily ration of food (25 g of dry diet per kg of body mass). When not fasting, cats were free in the animal facility room with other cats, and all were fed *ad libitum*. The housing rooms contained climbing frames, scratching posts and toys. Cats interacted daily with animal facility staff and/or researchers.

Our studies follow the ARRIVE 2.0 guidelines for animal studies (Percie du Sert et al., 2020). To minimize the number of animals, the same animals were used in several studies to address different scientific questions. Here we report new experimental results obtained in cats that also participated in previous studies (Audet et al., 2023; Farrell et al., 2015; Gregor et al., 2018; Harnie et al., 2024; Klishko et al., 2014, 2021; Lecomte et al., 2022, 2023; Maas et al., 2010; Mari et al., 2023; Mari et al., 2024; Merlet et al., 2022; Park et al., 2023).

Specimens and experimental subjects

This project involved three groups of animals. Fourteen forelimbs were harvested from 10 female cats (1–2 years, 4.5–5.5 kg) that had been euthanized by an overdose of pentobarbital (120 mg/kg, I.V., according to guidelines from the American Veterinary Medical Association) following unrelated experiments involving only the hindlimb. Of these limbs, six were used for muscle morphology, four were used to collect passive kinematics for joint centre estimation, and eight limbs were used for moment arm measurements. Segment lengths of the six morphology forelimbs are summarized in Table 1.

Forelimb kinematics and ground reaction forces during overground walking at self-selected speeds were recorded in a group of seven adult female cats (1–2 years, mass 3.20 $\pm$ 0.34 kg; Tables 2 and 3). Electromyographic activity (EMG) of forelimb muscles during treadmill walking at a speed of 0.4 m/s was recorded in a separate group of 16 adult female and male cats (1–2 years, mass 4.82 $\pm$ 0.99 kg, Table 4).

At the end of the study, the cats were euthanized by an overdose of pentobarbital (120 mg/kg, I.V., according to guidelines from the American Veterinary Medical Association).

Mathematical model

Strategy. The model includes 26 intrinsic muscles, subdivided to account for 40 tendons of insertion, with forces estimated by Hill-style models (Bunderson et al., 2010; Prilutsky et al., 2016) and rigid tendons, and afferent feedback estimated by Prochazka-style spindle and tendon organ models (Prochazka, 1999). Joint centres were defined by motion-captured passive mechanics and further refined to match measured wrist and elbow moment arms. Muscle attachment points were measured using a coordinate measuring machine (CMM) during dissection. A model was initially constructed in three dimensions, then reduced to a planar equivalent. Hill model parameters were estimated from architectural measurements. To further simplify calculations, muscles were lumped into nine functional group equivalents based on mechanical actions.

Recording of passive limb kinematics. The right forelimb of four specimens was skinned and disarticulated at the scapula within ~30 min after performing euthanasia and before establishment of rigor mortis. Self-tapping threaded rods were inserted into the scapula, humerus, ulna and radius, and a 2-mm rod was driven through the medial–lateral axis of the paw. A plastic tubing elbow was fixed to each rod, and 4-mm reflective spheres mounted at the ends of the elbows and the end of each rod to produce bone-fixed marker triads. The limb was then manipulated within the field of view of a six-camera Vicon motion capture system (Vicon Motion Systems Ltd, Yarnton, UK), with kinematic data collected at 100 Hz. Special attention was paid to moving each joint through a comfortable range of motion without imposing large forces or moments. Multiple recordings were made of each specimen, with some recordings emphasizing a single

Table 1. Segment lengths of forelimbs from which morphological characteristics were obtained (cm)

Cat	Scapula	Humerus	Radius	Carpals + metacarpals
Cat 1	6.65	9.49	8.84	3.09
Cat 2	7.26	10.39	9.30	3.59
Cat 3	7.22	10.16	9.35	3.23
Cat 4	7.28	10.05	9.06	3.27
Cat 5	7.31	10.07	9.40	3.53
Cat 6	7.04	9.56	9.07	3.29
Mean ± SD	7.13 ± 0.25	9.95 ± 0.36	9.17 ± 0.22	3.33 ± 0.19

articulation and some making an accordion-like motion to change all joint angles simultaneously.

Measurement of moment arms. Eight forelimbs from four specimens were used for moment arm measurements. These limbs were skinned and disarticulated at the scapula following resolution of rigor mortis. For wrist moment arms, self-tapping and threaded bone pins driven through the radius and ulna were used to immobilize the specimen. Silk sutures were tied to the distal tendons of the prime wrist movers (flexor carpi ulnaris, FCU; extensor carpi ulnaris, ECU; flexor carpi radialis, FCR; and extensor carpi radialis, ECR) routed along the respective muscle bellies, wrapped around the shafts of rotary potentiometers, and fixed to 500-g suspended weights. A dual-axis electrogoniometer was fixed to the paw and the forearm to record joint angles. The paw was then manipulated through flexion–extension and radial–ulnar deviation movements, while joint angles and tendon displacement were digitized. For elbow moment arms, the humerus was immobilized by bone pins, and sutures were connected to the triceps and biceps brachii tendons. Tendon-displacement *vs*. joint angle curves were fitted to cubic polynomials and differentiated to give quadratic moment arms (An et al., 1983; Young et al., 1993).

Joint centres. To capture 3-D kinematics of the forelimb, we defined seven rotational degrees of freedom or axes: three shoulder axes, elbow flexion–extension, radio-ulnar joint to capture pronation–supination, wrist dorsiflexion/plantarflexion, and wrist radial–ulnar deviation. Joint axes were identified by transforming the marker motion of each distal segment into a coordinate system defined by the marker triad of the adjacent proximal segment. An unconstrained optimization was used to determine the location (and axis orientation for hinge joints) of the joint centre which minimized deviation of the transformed data from the surface (cylinder or sphere) defined by the joint. These joint centres were transferred into the specimen-specific mathematical models, and the recorded motions were played back for validation.

Because of substantial noise in the kinematic data, specific inclusion criteria were applied to the kinematic datasets. The spatial distribution of each point was required to exceed 20° to ensure that the joint was in fact moved during the specific manipulation. Furthermore, in some specimens, it was apparent that a set of marker triads moved relative to the bones at some point between collection of the kinematic data and digitization of individual points of interest (marker triads, bony landmarks and muscle attachments), which prevented transformation of the joints proximal and distal to the corrupted marker into the anatomical coordinate system. This prevented accurate determination of joint centres for two elbows, two radio-ulnar and two wrist joints. Thus, the preliminary axes for each joint were ultimately based on only two specimens, but two different specimens depending on the joint.

Preliminary joint definitions were further refined based on measured moment arms. Constrained optimization was used to minimize the sum of square difference between the model and experimental moment arms for the biceps brachii and triceps muscles, subject to the constraints that the location of the elbow joint was not allowed to vary by more than 5 mm from the joint centre as defined by the kinematic data and the orientation was not allowed to vary by more than 5°.

The radial–ulnar articulation was refined to reduce the variation in wrist moment arms with supination. We performed constrained optimization minimizing the difference between flexion–extension moment arms at 0° and 90° of supination while constraining the orientation of the radial–ulnar hinge axis, which was allowed to vary by no more than 4° from the orientation obtained with kinematic data.

The wrist joint was refined by constrained optimization minimizing the difference between modelled and measured ECU, FCU, ECR and FCR moment arms where the location of the wrist joint was allowed to vary by no more than 5 mm from the joint centre as defined by the kinematic data and the orientation was allowed to vary by no more than 10°.

Table 2. Characteristics of cats participated in motion capture experiments

Cat	Sex	Mass (kg)	Scapula length (cm)	Upper arm length (cm)	Forearm length (cm)	Carpals + metacarpals length (cm)	Number of analysed cycles	Cycle duration (mean ± SD) (s)	Duty cycle (mean ± SD)
BL	F	3.00	6.50	8.75	8.90	3.4	35	0.695 ± 0.026	0.63 ± 0.01
IN	F	3.35	5.05	9.09	9.66	2.3	29	0.688 ± 0.030	0.65 ± 0.01
KA	F	3.15	5.30	9.55	8.91	3.0	13	0.634 ± 0.024	0.64 ± 0.01
MA	F	3.05	6.20	8.95	10.00	2.4	44	0.582 ± 0.021	0.63 ± 0.01
RY	F	2.80	5.75	10.00	10.00	2.05	19	0.867 ± 0.025	0.64 ± 0.01
SV	F	3.86	5.75	9.49	9.49	3.0	68	0.619 ± 0.003	0.65 ± 0.002
TU	F	3.20	5.85	9.10	9.30	2.15	3	0.747 ± 0.032	0.62 ± 0.02
Mean ± SD	—	3.20 ± 0.34	5.77 ± 0.49	9.28 ± 0.43	9.47 ± 0.46	2.61 ± 0.52	—	0.692 ± 0.093	0.64 ± 0.01

Note: Measurements of segment lengths were performed on sedated cats by an anthropometer. The number of cycles analysed corresponds to the maximum number of cycles analysed for a selected mechanical variable.

Muscle attachments. Anatomical data were collected from six specimens (Table 1). A set of rigid clamps was used to interlock the bone-mounted rods with the forelimb in a stance-like posture. The assembly was then immersed in 4% buffered formalin for 2–3 weeks. Care was taken not to displace or distort the marker triads, when present, which were used to align the kinematic data with the anatomical data. Following fixation, specimens were transferred to phosphate-buffered saline (PBS) and stored at 4°C between dissection sessions.

To collect muscle attachment points, each specimen was mounted within the workspace of a 5-axis CMM (Microscribe, Immersion Corporation, San Jose, CA, USA). The locations of fixed points on the immobilization framework were recorded, followed by locations of kinematic triads, bony landmarks and muscle origin, insertion and via points. Each of these points was digitized at least three times, with the specimen removed from its mounting and moved to a different region of the CMM workspace between measurements. Superficial muscles obscured the connections of deeper muscles. As each superficial muscle was fully digitized, it was carefully dissected and reserved for architectural measurements. Each specimen required four to six layers of dissection, depending on posture.

The repeated digital point recordings were aligned to a common reference frame by equiform transformation (Veldpaus et al., 1988). This transformation relies on the fixed points in the immobilization framework, which were common to all the recordings of a particular specimen. The aligned anatomical points were then averaged to define a specimen-specific model. Because the specimens were fixed in different postures, the specimen-specific models were segmented, and the segments were aligned by equiform transformation. The aligned segments were then averaged to produce the final anatomical dataset. Bony landmarks in each segment were used to define segmental coordinate systems.

Architectural measurements of muscles. Muscle–tendon units (MTU; each MTU included the muscle belly plus internal and external tendon) from four specimens (Table 1, cats 2, 3, 5, 6) were used for architectural measurements. Each muscle was cleaned of excess connective tissue, including external tendon, and fat and weighed. The length of muscle along its longest axis was measured with dial calipers and the surface pennation angle (α^P), the angle between the apparent muscle line of action and predominant fibre direction, was measured with a goniometer. Pennation angle measurements were taken from fascicles that were visually representative of the surface fascicles and located in the proximal, medial and distal portions of each muscle. These measurements were averaged within each muscle. Muscles were then digested for 2–5 days in 10% nitric acid and rinsed several times

Table 3. Inertial parameters of forelimb segments of seven cats for whom joint moments of force were computed (mean ± SD)

Parameter	Scapula	Upper arm	Forearm	Carpals	Digits
Centre of mass location (cm)	2.75 ± 0.24	4.53 ± 0.21	4.30 ± 2.1	1.37 ± 0.27	1.27 ± 0.41
Mass (g)	63.1 ± 4.0	81.0 ± 6.6	41.6 ± 3.3	7.5 ± 1.6	5.1 ± 1.3
Moment of inertia (g mm^2)	35,004 ± 2833	59,760 ± 9617	35,388 ± 4338	587 ± 179	—

Note: Segment inertial parameters were computed from cat mass and forelimb segment length using regression equations developed in Hoy & Zernicke (1985). Centre of mass location is determined from the proximal segment end. Moment of inertia is determined with respect to the medio-lateral axis at the segment centre of mass. Digits are considered a point mass, that is, there is no moment of inertia with respect to the digits centre of mass.

Table 4. Characteristics of cats participated in EMG recordings of forelimb muscles

Cat	Mass (kg)	Sex	Number of analysed cycles	Cycle duration (mean ± SD) (s)	Duty cycle (mean ± SD)
BE	5.10	Male	123	0.896 ± 0.118	0.70 ± 0.05
DE	4.65	Male	14	1.183 ± 0.058	0.74 ± 0.03
GR	4.80	Female	17	1.030 ± 0.107	0.71 ± 0.05
HO	5.90	Male	17	1.059 ± 0.089	0.77 ± 0.02
JA	6.10	Male	10	0.975 ± 0.179	0.72 ± 0.06
KA	4.00	Female	34	0.930 ± 0.056	0.71 ± 0.02
KI	5.60	Male	25	1.046 ± 0.120	0.72 ± 0.04
LIM	3.55	Female	54	0.908 ± 0.079	0.74 ± 0.03
LIS	3.15	Female	18	1.028 ± 0.198	0.69 ± 0.06
MO	5.34	Male	61	1.083 ± 0.116	0.69 ± 0.05
OS	6.30	Male	14	0.971 ± 0.043	0.74 ± 0.02
PA	3.99	Female	31	0.822 ± 0.078	0.70 ± 0.05
RI	4.80	Male	48	1.185 ± 0.185	0.75 ± 0.04
TOK	3.95	Female	31	1.092 ± 0.223	0.72 ± 0.08
TOR	6.00	Male	18	1.079 ± 0.127	0.75 ± 0.03
VE	3.87	Female	16	1.106 ± 0.158	0.74 ± 0.05
Mean ± SD	4.82 ± 0.99	—	—	1.025 ± 0.102	0.72 ± 0.02

in PBS. Bundles of muscle fibres were teased from the digested muscle, being careful to keep fascicles intact from proximal to distal tendons, and permanently mounted on glass slides. Between three and five fascicle bundles were collected from proximal, medial and distal portions of each muscle, or where muscles had a dramatic variation of fascicle length, from portions with shorter, longer and central fascicles. The length of each fascicle was measured with dial calipers and averaged within each muscle to determine the mean length. The sarcomere length of each bundle was determined by laser diffraction. The length of each fascicle was normalized to the optimal sarcomere length of 2.43 μm (Burkholder & Lieber, 2001), and the normalized fascicle lengths were averaged to give the optimal muscle fascicle length (L_0^{M}) for each muscle. PCSA was determined by the equation:

$$\mathrm{PCSA} = \frac{M^{\mathrm{m}} \cos\left(\alpha^{\mathrm{p}}\right)}{L_0^{\mathrm{M}} \rho^{\mathrm{m}}}, \tag{1}$$

where M^{m} is the muscle mass, α^{p} is the pennation angle, L_0^{M} is the optimal fascicle length and $\rho^{\mathrm{m}} = 1.056\ \mathrm{g/cm^3}$ is muscle density (Mendez and Keys, 1960).

Muscle force model. The tendon force (F^{T}) or the MTU force (F^{MTU}) was computed based on the phenomenological Hill-type muscle model as a function of muscle activation (A, $0 \leq A \leq 1$), muscle fascicle length (L^{M}) and velocity (V^{M}), pennation angle (α^{p}) and passive series and parallel elastic elements (eqns (2)–(6)) (He et al., 1991; Prilutsky et al., 2016). We simplified this model assuming that the series elastic component, including the internal and external tendon, is rigid. The tendon slack length of each MTU was selected such that the maximum muscle fascicle length during the walking cycle was 105% of the optimal fibre length (Burkholder & Lieber, 2001). The corresponding MTU length at this instant of the cycle was considered the optimal MTU length (L_0^{MTU}). The tendon slack length (L^{T}) was

computed as $L^{T} = L_0^{MTU} - L_0^{M}\cos(\alpha^{P})$. Forces produced by the tendon, contractile and parallel elastic elements of the Hill muscle model were computed as follows:

$$F^{T} = F^{MTU} = F^{M}\cos(\alpha^{P}), \quad (2)$$

$$F^{M} = F_{Max}^{M}\left[F^{CE}\left(L^{M}\right)F^{CE}\left(V^{M}\right)A + F^{PE}\left(L^{M}\right) + b^{M}V^{M}\right], \quad (3)$$

$$F^{CE}\left(L^{M}\right) = \exp\left(-\left|\frac{\left(L^{M}/L_0^{M}\right)^{\beta} - 1}{\omega}\right|^{\rho}\right), \quad (4)$$

$$F^{CE}\left(V^{M}\right) = \begin{cases} \frac{b_0 + b_1 V^{M}}{b_0 + V^{M}}, V > 0 \\ \frac{V_{max}^{M} + V^{M}}{V_{max}^{M} - a^{V}V^{M}}, V < 0 \end{cases}, \quad b_0 = V_{max}^{M}\frac{0.8}{a^{V}+1},$$

$$b_1 = \frac{1.8\left(V_{max}^{M} + b_0\right) - b_0}{V_{max}^{M}}, \quad (5)$$

$$F^{PE}\left(L^{M}\right) = k_1^{PE}/k_2^{PE}\left\{\exp\left(k_{PE2}\left[L^{M}/L_0^{M} - 1\right]\right) - 1\right\}, \quad (6)$$

where F^{M} is muscle fascicle force; $F_{Max}^{M} = 22.5 \cdot \mathrm{PCSA}$ is the maximum isometric muscle fascicle force at the optimum muscle fascicle length, PCSA is the muscle physiological cross-sectional area [in cm^2] and constant 22.5 [in N/cm^2] is muscle specific stress (Spector et al., 1980); $F^{CE}(L^{M})$ is the normalized isometric force-length relationship of the contractile element (muscle fascicles), eqn (4); $F^{CE}(V^{M})$ is the normalized force-velocity relationship of the contractile element, eqn (5); V_{max}^{M} is the muscle maximum shortening velocity [in m/s]; $F^{PE}(L^{M})$ is the normalized force-length relationship of the muscle parallel elastic element, eqn (6). Parameters of eqns (2)–(6) are summarized in Tables 5 and 6.

Afferent activity model. Firing rates of muscle spindle and Golgi tendon organ afferents during walking were estimated from the computed muscle fascicle length and velocity, muscle activation as well as MTU force using the regression equations developed in Prochazka & Gorassini (1998) and Prochazka (1999). The firing rates of spindle group Ia and II and Golgi tendon organ group Ib afferents were computed as follows:

$$R_{Ia} = 4.3V^{MTU^{0.6}} + 2\left(L^{MTU} - L_{0}^{MTU}\right) + 100A + R_{Ia_0}, \quad (7)$$

$$R_{II} = 13.5\left(L^{MTU} - L_{0}^{MTU}\right) + 20A + R_{II_0}, \quad (8)$$

$$R_{Ib} = 333F^{MTU}/F_{Max}^{MTU}, \quad (9)$$

where R_{Ia} is the firing rate of muscle spindle group Ia afferents (in Hz); V^{MTU} is MTU velocity (in mm/s); L_0^{MTU} is optimal MTU length (in mm); A ($0 \le A \le 1$) is normalized muscle activation; R_{Ia_0} is the mean of R_{Ia} over the cycle (in Hz); R_{II} is the firing rate of muscle spindle group II afferents (in Hz); R_{II_0} is the mean of R_{II} over the cycle (in Hz); R_{Ib} is the firing rate of Golgi tendon organ group Ib afferents (in Hz); $F_{Max}^{MTU} = F_{Max}^{M}\cos(\alpha^{P})$ is the maximum isometric MTU force (see eqn (2)). Note that the muscle activation term (A) in the equations of spindle afferent activities (R_{Ia} and R_{II}) accounts for fusimotor input assuming coactivation of alpha and gamma motoneurons as proposed in (Prochazka, 1999; Prochazka & Gorassini, 1998).

Reduction to planar model. We fitted a plane into 3D coordinates of attachment and via points of all studied forelimb muscles (Fig. 1A, 3D view; Supplement 1) by computing the first two principal components of the 3D coordinate data. We defined this plane as the forelimb sagittal plane. We projected muscle attachment and via points on this plane. We also computed the intersection points of the joint axes with the sagittal plane and defined these intersection points as joint centres in this plane. The sagittal plane representation of the forelimb segments (connecting joint centres) and muscles (connecting attachment and via points) is shown in Fig. 1A, sagittal view (Supplement 2). A minimum moment arm, or wrapping circle, was defined for each joint to prevent muscles from crossing the joint centre. All further analysis is based on this five degrees-of-freedom (DOF) model, in which the first two DOFs represent the horizontal and vertical coordinates of the shoulder marker (joint), and the other three DOFs represent the angles at the shoulder, elbow and wrist joints, as defined in Fig. 1, sagittal view.

Calculations of MTU lengths and moment arms during locomotion. We computed the instantaneous length of each MTU in locomoting cats from the experimental joint angles and morphological parameters of the MTU and joints. The morphological parameters included the distance of the MTU attachment point on the proximal (α_1) and distal (α_2) segment to the joint centre, the angle formed by the line from the attachment point to the joint centre and the proximal (φ_1) and distal (φ_2) segments, the radius of the joint spanned by a one-joint muscle (R_1) or the radii of the proximal (R_1) and distal (R_2) joints spanned by a two-joint muscle (Fig. 2). Additional geometric parameters necessary for calculating the MTU length and the corresponding equations are shown in Fig. 2. The equation parameters depend on the location of the MTU path with respect to one or two joints spanned by the muscle and on whether the MTU path wraps around the joints. Additional information about calculations of MTU lengths considering wrapping around joints and geometric parameters can be found in Table 5 and Supplement 3. The moment arm of the i-th MTU with

Table 5. Architectural properties of forelimb muscles

Muscle and primary joint action	Secondary joint action	Abbreviation	Muscle mass (g)	Optimal MTU length (mm)	Optimal fascicle length (mm)	Pennation angle (deg)	Tendon length (mm)	Tendon length/ optimal fascicle length ratio	PCSA (cm^2)	Fibre type: SO, FOG, FG (%)	nV^M_{max} (L^M_0/s)	Joint radius R_1 (mm)	Joint radius R_2 (mm)
Shoulder protractors		**Sh Prot**	**49.8**	**59.8**	**15.9**	**15**	**44.4**	**2.8**	**25.87**	**41.2,32.2, 26.5**	**11.0**	**7.94**	—
Acromiodel toideus	Shoulder abductor	AD	2.79 ± 0.47	59.1 ± 15.2	13 ± 2.9	31 ± 14	46.4	3.3	2.04 ± 0.6	21.9,78.1,0[g]	11.0	2.0	—
Coracobrac hialis	Shoulder adductor	CB	0.31 ± 0.04	31.0 ± 12.0	11±7.2	0 ± 0	23.4	1.5	0.34 ± 0.25	56,19,25[a]	10.2	5.0	—
Infraspinatus	Shoulder abductor	IF	13.2 ± 1.7	78.9 ± 4.9	18.4 ± 3.1	15 ± 10	59.7	3.1	6.62 ± 1.07	37,24,39[a]	11.6	3.0	—
Supraspinatus	—	SPS	17.2 ± 1.8	86.1 ± 4.2	27.2 ± 5.6	6 ± 3	59.7	2.2	5.94 ± 1.33	49,23,28[a]	10.6	21.9	—
Subscapularis	Shoulder adductor	SSC	15.4 ± 1.8	78.3 ± 5.1	13.7 ± 1.5	26 ± 6	66.4	4.8	10.25 ± 1.2	32,26,42[a]	12.0	6.2	—
Teres minor	—	TN	0.93 ± 0.22	32.2 ± 4.9	12.5 ± 3.8	12 ± 8	20.9	1.7	0.7 ± 0.16	51,23,25[a]	10.6	1.6	—
Shoulder retractors		**Sh Ret**	**12.01**	**71.4**	**39.5**	**4**	**32.0**	**0.8**	**2.7**	**21.9,78.1,0**	**11**	**1.84**	—
Spinodeltoideus	Shoulder abductor	SD	3.54 ± 1.01	72.1 ± 4.1	32.9 ± 3.5	1 ± 1	36.9	1.1	1.01 ± 0.4	21.9,78.1,0[g]	11	1.8	—
Teres major	—	TJ	8.5 ± 1.4	84.7 ± 2.6	46.1 ± 5.7	7 ± 5	36.8	0.8	1.69 ± 0.38	21.9,78.1,0[b]	11	3.5	—
Shoulder Protr-Elbow Flex		**Sh Prot-El Fl**	**5.9**	**70.5**	**25.1**	**10**	**45.8**	**1.8**	**2.27**	**20,21,59**	**11.9**	**10.0**	**5.30**
Biceps brachii	—	BB	5.9 ± 1.0	81.0 ± 8.7	25.1 ± 7.6	10 ± 10	53.9	2.2	2.27 ± 0.81	20,21,59[c]	11.9	10.0	5.3
Shoulder Retr-Elbow Ext		**Sh Ret-El Ex**	**22.9**	**98.8**	**23.9**	**13**	75.5	3.2	**9.2**	**26,17,57**	**11.4**	**4.40**	**11.90**
Triceps brachii longus	—	TLONG	22.9 ± 3.9	93.1 ± 8.1	23.9 ± 7.1	13 ± 11	66.4	2.8	9.2 ± 2.75	26,17,57[c]	11.4	4.4	11.9
Elbow extensors		**El Ext**	**18.5**	**69.7**	**29.1**	**10**	**41.0**	**1.4**	**5.58**	**55.3,13. 3,31.5**	**8.7**	**2.10**	—
Anconeus	Forearm pronator	ANC	2.04 ± 0.13	56.6 ± 8.8	20.1 ± 2.5	19 ± 5	38.7	1.9	0.94 ± 0.13	100,0,0[c]	4.7	2.4	—
Epitrochlearis	—	EPT	1.95 ± 0.51	66.5 ± 8.5	30.1 ± 3.6	0 ± 0	32.6	1.0	0.59 ± 0.16	26,17,57[g]	11.4	2.1	—
Triceps brachii lateralis	—	TLAT	9.0 ± 2.2	78.2 ± 5.6	36.8 ± 5.1	8 ± 3	38.4	1.0	2.3 ± 0.84	15,22,63[c]	12.3	5.8	—
Triceps brachii medialis	—	TMED	5.6 ± 0.4	83.8 ± 7.9	29.2 ± 3.8	11 ± 4	53.4	1.7	1.75 ± 0.21	80,14,6[c]	6.4	8.4	—

(*Continued*)

Table 5. (Continued)

Muscle and primary joint action	Secondary joint action	Abbreviation	Muscle mass (g)	Optimal MTU length (mm)	Optimal fascicle length (mm)	Pennation angle (deg)	Tendon length (mm)	Tendon length/ optimal fascicle length ratio	PCSA (cm^2)	Fibre type: SO, FOG, FG (%)	nV^M_{max} (L^M_0/s)	Joint radius R_1 (mm)	Joint radius R_2 (mm)
Elbow flexors	—	**El Fls**	**5.9**	**69.7**	**44.5**	**10**	**25.9**	**0.6**	**2.5**	**16.5,40.2, 43.2**	**12.2**	**3.20**	—
Brachioradialis	Forearm supinator	BCD	0.80 ± 0.21	136.7 ± 12.5	89.6 ± 9.1	0 ± 0	37.5	0.4	0.08 ± 0.03	13,19,67[a]	13.1	5.8	—
Brachialis	—	BR	3.47 ± 0.35	88.6 ± 6.0	32.4 ± 4.4	10 ± 4	52.9	1.5	0.99 ± 0.22	25,24,51[c]	11.4	6	—
Pronator teres	Forearm pronator	PT	1.62 ± 0.28	51.4 ± 12.3	11.5 ± 3.5	22 ± 4	34.9	2.6	1.43 ± 0.73	11.5,77.5, 11.5[b]	12	4.2	—
Elbow flexor–wrist dorsiflexors		**El Fl-Wr dFl**	**11.8**	**76.5**	**27.4**	**7**	**49.3**	**1.8**	**4.35**	**4,30.8,65.2**	**13.3**	**5.40**	**3.50**
Extensor carpi radialis	—	ECR	3.88 ± 0.66	98.3 ± 19.4	47.3 ± 35.3	15 ± 0	48.5	0.7	0.97 ± 0.59	4,41.9,53.9[d]	13.1	5.5	3.5
Extensor digitorum communis	—	EDC	1.98 ± 0.17	85.8 ± 3.7	22.5 ± 6.7	5 ± 4	62.3	3.0	0.85 ± 0.21	4,28,68[e]	13.3	5.3	6.1
Wrist plantarflexors		**Wr pFl**	**65.4**	**79.8**	**13.2**	**8**	**66.7**	**5.1**	**36.97**	**20.1,30.4, 49.4**	**11.7**	**2.70**	—
Flexor carpi radialis	—	FCR	1.26 ± 0.17	83.4 ± 15.7	14.3 ± 2.3	6 ± 1	79.1	5.7	0.85 ± 0.14	38.1,29.4, 32.3[f]	10.1	2.7	—
Flexor carpi ulnaris	—	FCU	4.01 ± 0.32	104.0 ± 2.6	11.1 ± 1.1	11 ± 2	93.0	8.1	3.3 ± 0.31	42.4,24.2, 33.4[f]	9.7	5.6	—
Flexor digitorum profundus	—	FDP	9.27 ± 2.00	103.9 ± 6.1	21.5 ± 2.7	7 ± 12	83.3	3.8	3.97 ± 1.07	8.1,34.6,57.2[f]	12.8	5.5	—
Flexor digitorum superficialis	—	FDS	0.18 ± 0.05	29.1 ± 4.3	5.85 ± 2.2	3 ± 3	22.8	3.4	0.29 ± 0.07	26.8,29.2, 43.9[g]	11.1	2.7	—
Palmaris longus	—	PL	2.61 ± 0.55	101.8 ± 22.2	10.9 ± 1.4	14 ± 6	101.8	8.8	2.36 ± 0.61	18.7,28.7, 52.6[f]	11.9	6.3	—
Wrist dorsiflexors		**Wr dFl**	**1.11**	**78.4**	**21**	**1**	**57.4**	**2.7**	**0.25**	**2,55,43**	**13.2**	**2.40**	—
Extensor pollicis longus	—	EPL	0.55 ± 0.07	86.1 ± 8.1	21 ± 6	1 ± 1	62.5	3.0	0.25 ± 0.08	2,55,43	13.2	2.4	—

Note: Tendon length at the optimal MTU length was computed using optimal MTU length (L_0^{MTU}), optimal fascicle length (L_0^M) and pennation angle (α^P) as $L_0^{MTU} - L_0^M \cos(\alpha^P)$. Five compartments of flexor digitorum profundus, four compartments of flexor digitorum superficialis, five compartments of palmaris longus and two compartments of extensor pollicis longus (see Fig. 1B) are combined in the corresponding single muscles; SO, FOG and FG are percentage of slow oxidative, fast oxidative glycolytic and fast glycolytic fibres in the muscle; nV^M_{max} is muscle maximum shortening velocity normalized to the optimal muscle fascicle length (L_0^M). nV^M_{max} was estimated from the percentage of SO, FOG and FG fibres in the muscles as $nV^M_{max} = (4.65 \cdot SO + 12.8 \cdot FOG + 14.0 \cdot FG)/(SO + FOG + FG)$, where constants 4.65, 12.8 and 14.0 are maximum shortening velocities [in L_0^M/s] of SO, FOG and FG muscle fibres measured or estimated in (Spector et al., 1980; Scott et al., 1996; Singh et al., 2002). When no information on fibre composition in a cat forelimb muscle was available, we used this information from other mammalian species. [a]Taken from *Macaca* (Singh et al., 2002); [b]taken from rabbit (Prado et al., 2005); [c]taken from cat (Collatos et al., 1977); [d]taken from rat (Watt et al., 1982); [e]taken from mouse (Mathewson et al., 2012); [f]taken from cat (Gonyea et al., 1981); [g]taken from the synergistic muscles due to lack of information in the literature. Values of morphological variables in bold font indicate values computed by the optimization algorithm (see Methods, eqns (6)–(11)) or estimated from the literature for the nine equivalent MTU groups.

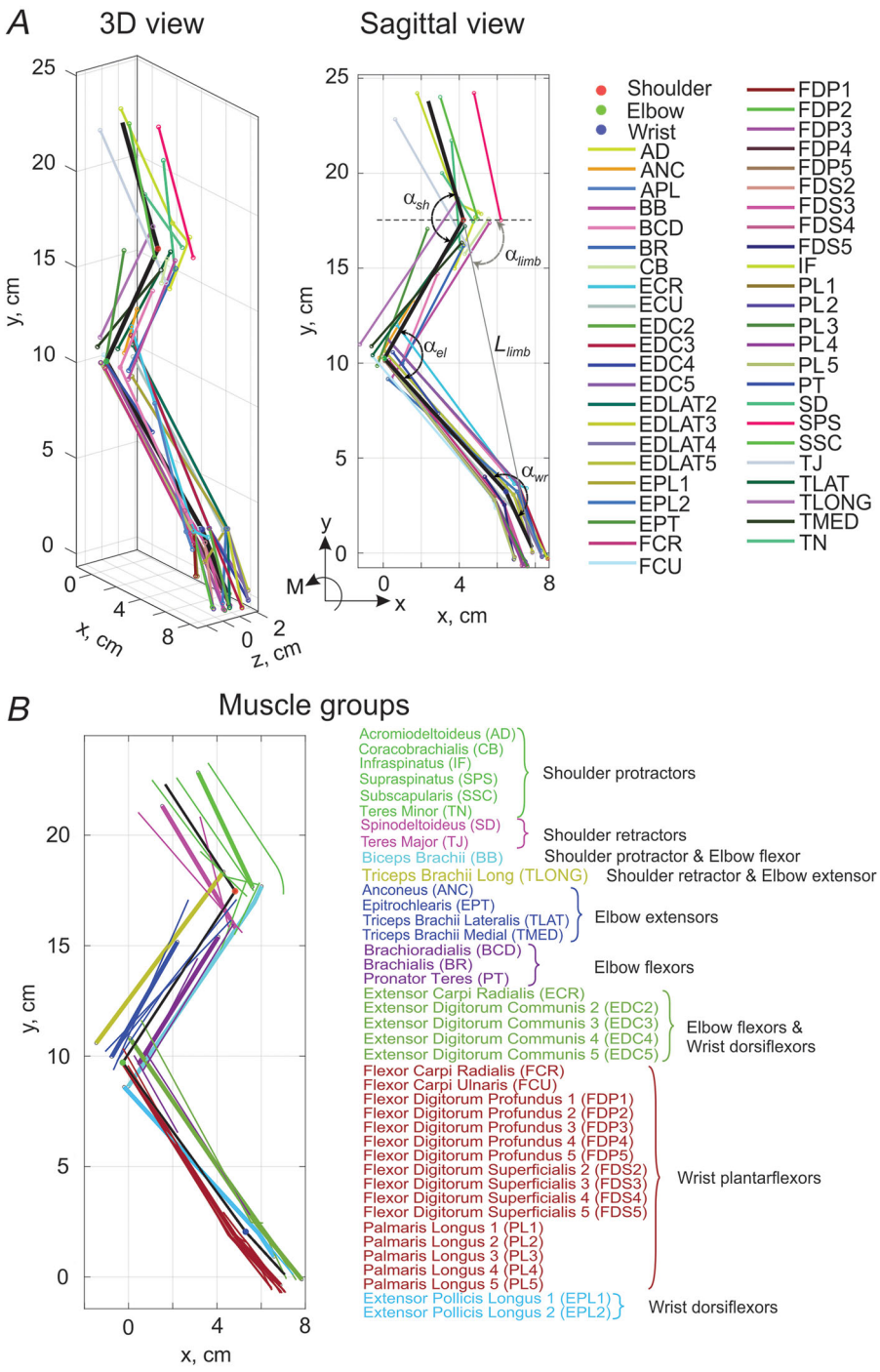

Figure 1. Schematic of cat forelimb musculoskeletal model
Black lines designate the scapular, upper arm, forearm and carpals. Coloured circles indicate locations of the shoulder, elbow and wrist centres. α_{sh}, α_{el} and α_{wr} define shoulder, elbow and wrist joint angles. Open small circles indicate origin, via points and attachment of muscle–tendon units (MTUs). Coloured lines connecting the origin and attachment points correspond to forelimb MTUs. *A*, 3D and 2D sagittal plane views of cat forelimb with 46 MTUs. Thin grey line connecting the shoulder centre and the most distal carpals point define the forelimb length (L_{limb}); angle α_{limb} defines limb orientation. *B*, results of the cluster analysis of mechanical actions of 40 MTUs based on their maximum moment of force at joints in the sagittal plane. Six MTUs whose major mechanical action is outside the sagittal plane are excluded from cluster analysis. Thin and thick lines of the same colour correspond to individual MTUs and their equivalent MTU with the same mechanical action at a joint, respectively (see text for details). [Colour figure can be viewed at wileyonlinelibrary.com]

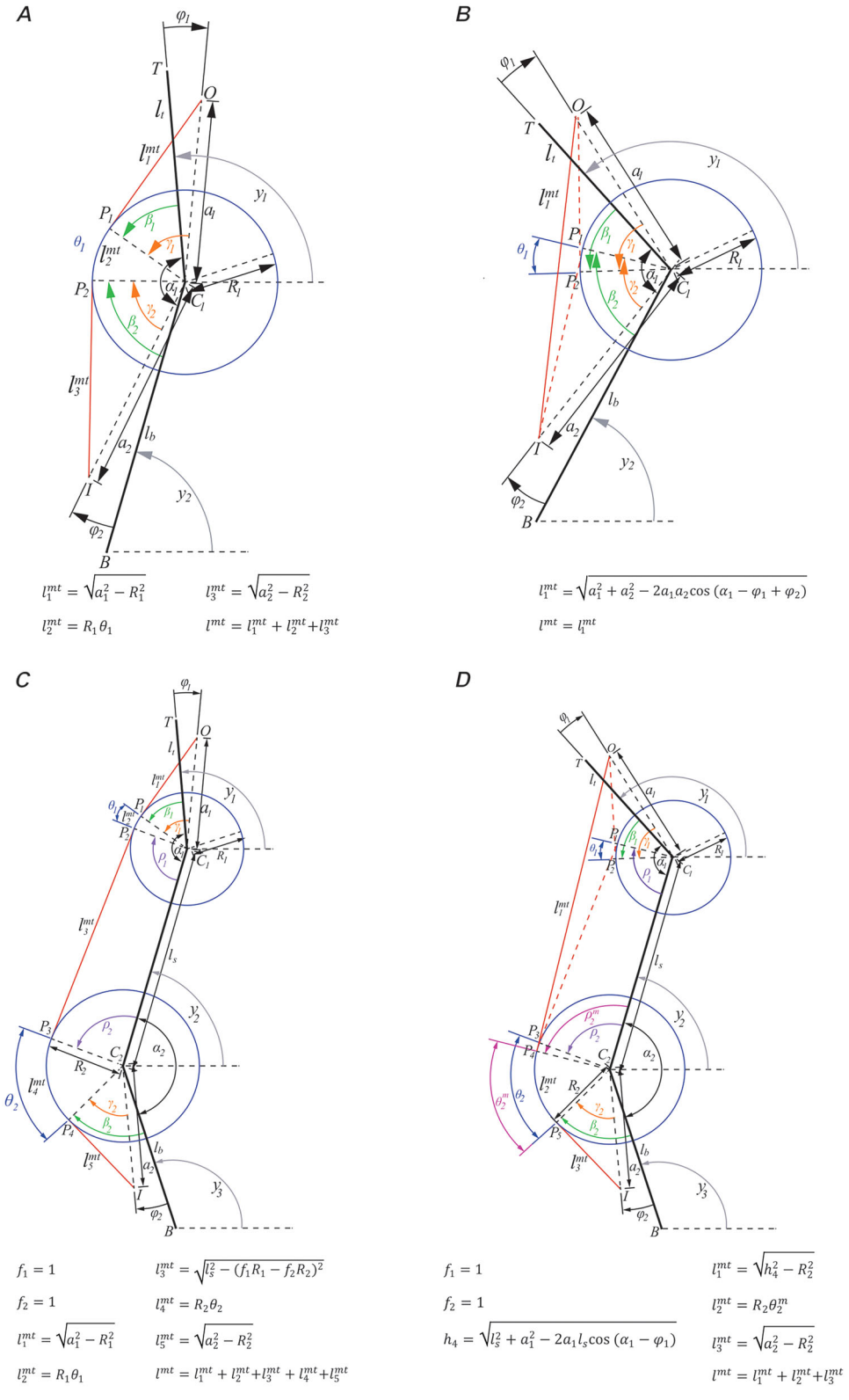

Figure 2. Schematic diagrams demonstrating calculations of the path, length and moment arms of one- and two-joint MTUs as functions of the joint angles and geometric parameters of the MTU and joint
O and *I* are points of MTU origin and insertion; α_1 and α_2 are distances from the joint centre to *O* and *I*, respectively; φ_1 and φ_2 are angles formed by the limb segment and lines from the joint centre to *O* and *I*, respectively; R_1 and R_2 are joint radii. If the MTU path is not in contact with joint surface, defined by the circle around the joint centre, MTU length is defined as the distance between *O* and *I*. If the MTU path wraps around the joint surface, the total

Table 6. Selected parameters of the muscle model

Muscle force relationship	Equation	Parameter	Value
Force–velocity relationship of passive muscle	3	b^{M}	0.02 N s/m
Normalized isometric force–length relationship of contractile component, $F^{CE}(L^{M})$	4	ω	0.55
		ρ (for $L^{T}/L_0^{M} \leq 1$)	6.0
		ρ (for $L^{T}/L_0^{M} > 1$)	3.0
		β	1.55
Normalized force–length relationship of passive elastic element, $F^{PE}(L^{M})$	6	k_1^{PE}	0.0075
		k_2^{PE}	11.6

MTU length is the sum of the three lengths: $l^{mt} = l_1^{mt} + l_2^{mt} + l_3^{mt}$ (see figure for definitions of these and other parameters). MTU moment arm at a joint is computed as the shortest distance from the MTU path to the joint centre. *A* and *B*, path definition for one-joint MTUs located posterior to the joint centre with wrapping or without wrapping around the joint. *C* and *D*, path definition for two-joint MTUs located posterior to the joint centres with different combinations of wrapping around the two joints. [Colour figure can be viewed at wileyonlinelibrary.com]

respect to the j-th joint, $r_{i,j}$, was computed as the derivative of the MTU length over the joint angle.

Reduction to functional groups. We classified muscles based on their maximum moment of force produced in the walking cycle. The maximum moment of force was computed for each percentage of the cycle as the product of the MTU moment arm and MTU force assuming maximum muscle activation ($A = 1$). MTUs were classified into functional groups using the k-means clustering algorithm of MATLAB (The MathWorks, Inc., Natick, MA, USA). The equivalent mass and PCSA of each functional group were computed as the sum of the masses and PCSAs of the MTUs within each cluster. The other morphological parameters (Fig. 2, Table 7) of each functional group were determined by minimizing the difference between the total maximum moment of MTUs in a cluster and the moment of the equivalent MTU produced during the walking cycle (optimization function *fmincon* in MATLAB):

$$\min\ Z_1 = \left[\sum_{t=0}^{100}\left(\tau_{kt}^{Eq} - \tau_{kt}^{Cl}\right)/\mathrm{SD}^{\tau_k^{Cl}}\right]^2, \tag{10}$$

subject to constraints:

$$\min_{i_k}\left(a_{i_k}^{Cl}\right) \leq a_k^{Eq} \leq \max_{i_k}\left(a_{i_k}^{Cl}\right) \tag{11}$$

$$\min_{i_k}\left(\varphi_{i_k}^{Cl}\right) \leq \varphi_k^{Eq} \leq \max_{i_k}\left(\varphi_{i_k}^{Cl}\right) \tag{12}$$

$$\min_{i_k}\left(R_{i_k}^{Cl}\right) \leq R_k^{Eq} \leq \max_{i_k}\left(R_{i_k}^{Cl}\right) \tag{13}$$

$$R_k^{Eq} \leq a_k^{Eq}, \tag{14}$$

$$\mathrm{mean}\left[\min_{i_k}\left(L_{i_k}^{M_{Cl}}\right)\right] \leq L_k^{M_{Eq}} \leq \mathrm{mean}\left[\max_{i_k}\left(L_{i_k}^{M_{Cl}}\right)\right] \tag{15}$$

where τ_{kt}^{Cl} and τ_{kt}^{Eq} are the total moment of all MTUs in k-th cluster at the t-th instant of the normalized cycle time and the moment of the equivalent MTU substituting the total moment of the same MTU cluster at time instant t, respectively; $\mathrm{SD}^{\tau_k^{Cl}}$ is the standard deviation of the total MTU cluster moment computed across all MTUs in the cluster at time t; $a_{i_k}^{Cl}$ is the distance from an attachment point to the joint centre of i-th MTU of cluster k (note that each MTU has two attachment points, Fig. 2); a_k^{Eq} is the distance from an attachment point to the joint centre of the equivalent MTU for cluster k; $\varphi_{i_k}^{Cl}$ is the angle between the segment line and the line between the joint centre and an attachment point of i-th MTU of cluster k (each MTU has two such angles, Fig. 2); $\varphi_{i_k}^{Eq}$ is the angle between the segment line and the line between the joint centre and an attachment point of the equivalent MTU of cluster k; $R_{i_k}^{Cl}$ is the joint radius of individual i-th MTU in k-th cluster at a joint this MTU spans; R_k^{Eq} is the joint radius of the equivalent MTU for cluster k at a joint spanned by this MTU; $L_{i_k}^{M_{Cl}}$ and $L_k^{M_{Eq}}$ are length of i-th MTU in cluster k and length of the equivalent MTU for cluster k in the walking cycle.

Gait analysis and inverse dynamics

Strategy. Overground walking kinematics were recorded by infrared motion capture and ground reaction forces were measured by force platforms. Muscle activations during walking were estimated by static optimization with a minimum fatigue cost function (Crowninshield & Brand, 1981). Estimation was performed for both the fully redundant, 40-MTU model and the simplified, nine-functional group model.

Table 7. Geometric parameters of nine forelimb equivalent MTUs representing sagittal plane actions of the corresponding individual MTUs with the same actions at the joints

Muscle	a_1 (cm)	a_2 (cm)	φ_1 (rad)	φ_2 (rad)	R_1 (cm)	R_2 (cm)
Shoulder protractor	5.64	0.795	−0.277	2.392	0.794	—
Shoulder retractor	5.08	1.67	0.128	0.595	0.184	–
Shoulder protractor–elbow flexor	1.22	1.11	−1.969	−0.400	1.00	0.53
Shoulder retractor–elbow extensor	1.02	1.49	−0.046	−2.832	0.44	1.19
Elbow extensor	6.00	0.56	0.155	−2.691	0.21	—
Elbow flexor	7.15	0.74	−0.070	0.899	0.32	—
Elbow flexor–wrist dorsiflexor (OV)	1.14	9.51	0.287	0.065	0.54	0.35
Elbow flexor–wrist dorsiflexor (VI)	0.61	3.33	−1.531	0.126		
Wrist plantarflexor (OV)	0.64	9.63	−0.047	−0.052	0.27	—
Wrist plantarflexor (VI)	0.52	2.89	1.282	−0.163		
Wrist dorsiflexor (OV)	1.11	9.89	−0.571	0.044	0.24	—
Wrist dorsiflexor (VI)	0.601	1.71	−2.333	0.115		

Note: The geometric parameters are explained in Fig. 2. The MTU paths of the elbow flexor–wrist dorsiflexor, wrist plantarflexor and wrist dorsiflexor consist of two lines connected by a via point (designated by V). The first line connects the point of origin (O) with V, and the second line connects V with the point of insertion (I).

Recording and analysis of forelimb locomotor kinematics and ground reaction forces. Seven cats (Tables 2 and 3) were trained to walk at self-selected speeds on a Plexiglas enclosed walkway with three embedded small force platforms (Bertec Corporation, Columbus, OH, USA) using food rewards and affection. After training for 2–4 weeks, animals were sedated (dexmedetomidine, 40–60 μg/kg, I.M.) and shaved. In the subsequent 2 weeks, we recorded full-body kinematics – 3D coordinates of 28 small reflective markers on major hindlimb and forelimb joints, the scapulas, the pelvis and the head (6-camera Vicon motion capture system, sampling frequency 120 Hz). We also recorded the three components of ground reaction forces applied to each hindpaw and forepaw as well as the coordinates of the force vector application at a sampling frequency of 360 Hz (Farrell et al., 2014; Klishko et al., 2014). We attached the reflective markers using double-sided adhesive tape on the following bone landmarks of the left and right forelimbs: intersection of the vertebral border and tuberosity of the spine on the scapula (the point approximating halfway between scapula cranial and caudal angles), humerus greater tubercle, humerus lateral epicondyle, ulna styloid process, lateral metacarpophalangeal joint (MCP) and distal phalanx of the 5th digit. After low-pass filtering recorded marker coordinates (4th order, zero-lag Butterworth filter, cutoff frequency 5–7 Hz), the coordinates of the elbow joint were recalculated by triangulation using coordinates of the humerus greater tubercle and ulna styloid process and segment lengths of the upper arm and forearm (Table 2) to reduce skin movement artefacts. An example of recorded full-body kinematics (3D coordinates of 28 reflective markers) and three components of the ground reaction force vectors applied to fore- and hind-limbs can be found in Supplement 4.

We computed the moment of force (resultant muscle moment, τ_j) at j-th joint in the sagittal plane using 2D Newton–Euler equations of motion of each forelimb segment distal to the joint, the recorded marker coordinates and ground reaction forces as well as the segment inertia parameters (mass, centre of mass location, moment of inertia with respect to the centre of mass, Table 3 (Farrell et al., 2014; Prilutsky et al., 2005)).

We identified individual locomotor cycles from successive swing onsets. The swing onset (stance offset) and swing offset (stance onset) were defined based on the relative horizontal displacement of the forepaw with respect to the shoulder, the method demonstrating the smallest random error of phase detection for the hindlimb (Pantall et al., 2012).

Implantation of EMG electrodes and recording and analysis of EMG activity. EMG activity of selected

forelimb muscles was recorded in 16 cats walking on a tied-belt treadmill with speed of 0.4 m/s. These animals were also used in other studies addressing different scientific questions (Audet et al., 2023; Harnie et al., 2024; Lecomte et al., 2022, 2023; Mari et al., 2023; Mari et al., 2024; Merlet et al., 2022). Before surgery, the cat was sedated with an intramuscular injection of a cocktail containing butorphanol (0.4 mg/kg), acepromazine (0.1 mg/kg) and glycopyrrolate (0.01 mg/kg) and inducted with another intramuscular injection (0.05 ml/kg) of ketamine (2.0 mg/kg) and diazepam (0.25 mg/kg) in a 1:1 ratio. The fur overlying the forelimbs and top of the head was shaved and the skin cleaned with chlorhexidine soap. Implantation surgeries were performed under aseptic conditions and general anaesthesia with isoflurane (1.5–3.0%) and O_2 delivered with a flexible endotracheal tube. The depth of anaesthesia was confirmed by testing a withdrawal response to applying pressure to a paw. Body temperature was monitored and maintained at 37 ± 0.5°C using a water-filled heating pad under the animal and an infrared lamp placed ∼50 cm above it. Pairs of Teflon-insulated multistrain fine wires (AS633; Cooner Wire Co., Chatsworth, CA, USA) were subcutaneously passed from two head-mounted 34-pin connectors (Omnetics Connector Corp., Minneapolis, MN, USA) to the muscles of interests. Two wires, stripped of 1–2 mm of insulation, were sewn into the belly of selected forelimb muscles for bipolar recordings. The head-mounted connectors were fixed to the skull using dental acrylic and four to six screws. Seven forelimb muscles were implanted bilaterally: supraspinatus (shoulder protractor), biceps brachii (shoulder protractor and elbow flexor), triceps brachii long head (shoulder retractor and elbow extensor), triceps brachii lateral head (elbow extensor), pronator teres (shoulder flexor and forearm pronator), brachialis (elbow flexor) and extensor carpi radialis (elbow flexor and wrist dorsiflexor). Electrode placement was verified during surgery by stimulating each muscle through the appropriate head connector channel. The skin was closed using subcuticular sutures (monocryl 4–0, Ethicon) followed by cutaneous sutures (monocryl 3–0, Ethicon). At the end of surgery, an antibiotic (cefovecin, 8 mg/kg) and a fast-acting analgesic (buprenorphine, 0.01 mg/kg) were injected subcutaneously. A fentanyl (25 μg/h) patch was taped to the back of the animal 2–3 cm rostral to the base of the tail for prolonged analgesia, which was removed 4–5 days later. After surgery, cats were placed in an incubator and closely monitored until they regained consciousness. Another dose of buprenorphine was administered ∼7 h after surgery. At the end of experiments, cats were anaesthetized with isoflurane (1.5–3.0%) and O_2 before receiving a lethal dose of pentobarbital (120 mg/kg) through the left or right cephalic vein. Cardiac arrest was confirmed using a stethoscope to determine the death of the animal.

During experiments, EMG signals were pre-amplified (×10, custom-made system), bandpass filtered (30–1000 Hz) and amplified (100–5000×) using a 16-channel amplifier (model 3500; AM Systems, Sequim, WA, USA). EMG data were digitized (5000 Hz) with a National Instruments (Austin, TX, USA) card (NI 6032E), acquired with custom-made acquisition software and stored on computer. Recorded EMG signals were full-wave rectified and low-pass filtered (Butterworth, zero lag 4th order filter, 10 Hz cutoff frequency). Locomotion cycle durations were identified for each forelimb as the time between swing onset and stance offset events. These time events were obtained from bilateral video recordings made by two cameras (Basler AcA640-100 G) at 60 frames per second with a spatial resolution of 640×480 pixels. A custom-made program (LabView, National Instruments) acquired the video images and synchronized them with EMG data. Low-pass filtered EMG signals were normalized to the peak filtered EMG across all cycles within the cat and muscle and then time-normalized to the duration of the cycle.

Estimation of muscle activation. To better understand forelimb locomotor functions, we computed patterns of muscle activation during the walking cycle using static optimization (Anderson & Pandy, 2001; Crowninshield & Brand, 1981; Prilutsky et al., 1997). Subject-specific models were generated for each animal by segment-length scaling of the planar model. The static optimization problem for each normalized cycle time instant was formulated as follows:

$$\min Z_2 = \sum_{i=0}^{N} \left(F_i^{\mathrm{MTU}}/\mathrm{PCSA}_i\right)^3, \tag{16}$$

subject to constraints

$$\tau_j - \sum_{i=1}^{N_j} d_{ji} F_i^{\mathrm{MTU}} = 0, \tag{17}$$

$$0 \leq A_i \leq 1, \tag{18}$$

where Z_2 is a cost function of minimum fatigue (Crowninshield & Brand, 1981); j indicates joint ($j = 1$, 2, 3 are wrist, elbow and shoulder, respectively); τ_j is the resultant moment of force averaged across all cycles of all cats for which we recorded kinematics and ground reaction forces and determined the segment inertial properties (Table 3); d_{ji} is the mean moment arm of the i-th MTU with respect to the j-th joint determined from the model geometry (Fig. 2); F_i^{MTU} is the force of i-th MTU that depends on muscle activation A_i, muscle fascicle pennation angle, length and velocity (eqns (2)–(6)). We used constrained optimization (function *fmincon* in MATLAB) to find the optimal muscle activations at each

time instant of the normalized cycle time starting from random initial activation values. The optimal activations were found for the two forelimb models, with all 40 MTU units and with the reduced number of equivalent MTU units each representing the functional cluster.

Estimation of spatiotemporal activity of cervical motoneuronal pools and their proprioceptive inputs during walking. Muscle nerves originating in cervical segments of the spinal cord consisting of axons from motor and proprioceptive sensory neurons innervate forelimb MTUs. There is a well-established anatomical organization of motoneuronal pools of forelimb muscles along the rostral–caudal direction of cervical spinal segments with proprioceptive afferents connecting to motoneurons of the parent muscles and, to a lesser extent, their synergists (Fritz, Illert, Reeh, 1986; Fritz, Illert, Saggau, 1986; Levine et al., 2012; Sterling & Kuypers, 1967a,b). This anatomical organization allows for evaluation of spatiotemporal activity of motoneurons during a locomotor cycle based on recorded or computed muscle activity as was done for the lumbar motor pools of locomoting cats (Yakovenko et al., 2002), for the entire spinal cord of humans (Ivanenko et al., 2006) and for proprioceptive inputs to cervical spinal segments during arm reaching and grasping in monkeys (Kibleur et al., 2020).

We used this approach to map the computed activation of forelimb MTUs (eqns (16)–(18)) and their proprioceptive activity (eqns (7)–(9)) during locomotion onto cervical spinal segments. We used available data on the distribution of motor pools of cat forelimb muscles in spinal segments C3 through T1 from Fritz, Illert, Reeh (1986), Fritz, Illert, Saggau (1986) and Horner & Kummel (1993). Because the cat data were missing for the BB, TLONG, FDS and EPL MTUs (MTU abbreviations are defined in Fig. 1 and Table 5) in the mentioned studies, we approximated their motor pool localizations using data on arm motor pools in monkeys (Jenny & Inukai, 1983; Kibleur et al., 2020). Since we could not find reliable data on MTUs CB, ANC, EPT, TLAT, TMED and BR, we approximated their motor pool localizations by the mean values of their synergistic MTUs. To quantify the distribution of motor pools along the spinal segments from published distribution histograms, we digitized them using GetData Graph Digitizer 2.26 software (Informer Technologies, Inc., Los Angeles, CA, USA) and then computed the total histogram area and the area corresponding to each spinal segment. The resulting proportions of motoneurons for each MTU in each cervical spinal segment are shown in Table 8. Assuming that motoneuronal pools of forelimb muscles and their proprioceptive inputs have the same rostro-caudal spinal distribution (Levine et al., 2012; Sterling & Kuypers, 1967a,b), we computed motor and sensory neuronal activities exiting and entering each spinal segment at each percentage of the locomotor cycle as follows (Kibleur et al., 2020):

$$a_{k,x} = \frac{\sum_{i=0}^{N^{\mathrm{MTU}}} \omega_i^k \, R_{x,i}}{\sum_{i=0}^{N^{\mathrm{MTU}}} \omega_i^k}, \; x = A,\ \mathrm{Ia},\ \mathrm{II},\ \mathrm{Ib} \qquad (19)$$

where $a_{k,x}$ is activity of type x in the k-th spinal segment; $R_{x,i}$ is the normalized motoneuronal activity or the firing rate of the proprioceptive afferents of type x of the i-th MTU; and ω_i^k is the proportion of i-th MTU's motoneurons in or its afferents projecting to the k-th spinal segment.

Statistical analysis

Comparisons between the functional groups of MTUs were made for individual morphological characteristic using a one-way analysis of variance (Statview 4.0, Abacus concepts, Inc., Berkeley, CA, USA), and in the case of a significant statistical value ($P < 0.05$), Fisher's protected least significant difference (PLSD) *post hoc* test was performed between pairs of functional groups.

Results

Forelimb morphology

The 3D musculoskeletal model of the cat forelimb and its 2D sagittal plane version are shown in Fig. 1A. The model includes four body segments (scapula, upper arm, forearm and carpals), three joints (shoulder, elbow and wrist) and MTUs of 46 muscles. For analysis of a muscle's motor and sensory functions during locomotion in the sagittal plane, we selected 40 MTUs (Fig. 1B), because the remaining six MTUs have negligible moments of force production in the sagittal plane. The six muscles excluded from the sagittal plane analysis were abductor pollicis longus (APL, wrist abductor), extensor carpi ulnaris (ECU, wrist dorsiflexor), and four compartments of extensor digitorum lateralis (EDLAT2, EDLAT3, EDLAT4, EDLAT5, wrist dorsiflexors).

Table 5 shows forelimb architectural measures of muscles of the 2D model (Fig. 1B). The forelimb MTUs in Table 5 are classified by functional groups and vertically arranged from proximal to distal. Qualitatively, the forelimb is more complex than the hindlimb, with substantially more and denser connective tissue and compartmentalization. The cat forelimb possesses many complex, multi-pennate muscles (see Fig. 1A and Table 5), unlike the more fusiform, uni-pennate muscles typically found in the cat hindlimb (Sacks & Roy, 1982). In addition, forelimb MTUs tend to have shorter tendons, with fibres inserting near the distal joint.

Table 8. Proportional distribution of the motor neurons of forelimb muscles in spinal cord segments

Muscle–tendon unit	Number of motoneurons	C5	C6	C7	C8	T1
Shoulder protractors						
AD	256	0.06	0.87	0.07	0	0
CB[b]	—	0.04	0.75	0.21	0	0
IF	536	0.06	0.65	0.29	0	0
SPS	849	0.07	0.78	0.15	0	0
SSC	874	0.02	0.65	0.33	0	0
TN	120	0.01	0.78	0.21	0	0
Total	2635					
Shoulder retractors						
SD	196	0	0.67	0.33	0	0
TJ	504	0	0.01	0.99	0	0
Total	700					
Sholder protractor–elbow flexor						
BB[a]	1051	0.37	0.40	0.19	0.04	0
Sholder retractor–elbow extensor						
TLONG[a]	—	0	0	0.26	0.52	0.22
Elbow extensors						
ANC[b]	—	0	0	0.26	0.52	0.22
EPT[b]	—	0	0	0.26	0.52	0.22
TLAT[b]	—	0	0	0.26	0.52	0.22
TMED[b]	—	0	0	0.26	0.52	0.22
Elbow flexors						
BCD	77	0	0.81	0.19	0	0
BR[b]	147	0	0.42	0.56	0.03	0
PT	216	0	0.01	0.94	0.05	0
Total	440					
Elbow flexors–wrist flexors						
ECR	589	0.09	0.32	0.59	0	0
EDC	363	0	0	0.01	0.63	0.36
Total	952					
Wrist extensors						
FCR	196	0	0	0	0.59	0.41
FCU	369	0	0	0	0.72	0.28
FDP1	109	0	0	0	0.66	0.34
FDP2	142	0	0	0	0.67	0.33
FDP3	120	0	0	0.02	0.56	0.42
FDP4	208	0	0	0	0.43	0.57
FDP5	158	0	0	0	0.52	0.48
FDS[b]	—	0	0	0	0.59	0.41
PL	285	0	0	0	0.57	0.43
Total	1587					
Wrist flexors						
EPL[b]	—	0.03	0.06	0.13	0.50	0.28

Notes: For muscle abbreviations see Fig. 1. Proportional distributions of motor neurons in the cervical cord segments were estimated based on the histograms of motor nuclei of cat forelimb muscles from Fritz, Illert, Reeh (1986), Fritz, Illert, Saggau (1986) and Horner & Kummel (1993).

[a]Due to lack of information in the literature, the proportional distributions of these motor pools were taken from monkey (Jenny & Inukai, 1983).

[b]Due to lack of information in the literature, the proportional distributions of these muscles were taken from the mean of their synergic muscles. MTU abbreviations are defined in Fig. 1 and Table 5.

Figure 3 shows select morphological characteristics of forelimb MTUs combined with respect to their actions in 3D (Fig. 1A). Muscle masses ranged from 0.18 ± 0.05 g for FDS to 22.9 ± 3.9 g for TLONG. As shown in Fig. 3A, muscle mass varied significantly among functional groups ($P < 0.001$), with greater and smaller masses concentrated in the proximal and distal limb, respectively. The shoulder protractors had the greatest mass (17.2 ± 1.8 g), followed by the shoulder adductors (10.3 ± 7.9 g) and elbow extensors (8.8 ± 8.5 g). These groups were significantly larger than the forearm supinator (0.86 ± 0.16 g), forearm pronator (1.86 ± 0.29 g), wrist dorsiflexor (1.69 ± 0.95 g) and wrist abductor (1.83 ± 0.24 g) groups.

The calculated PCSA ranged from 0.08 ± 0.03 cm^2 (BCD) to 10.25 ± 1.19 cm^2 (SSC) (Table 5) with a proximo-distal gradient that was qualitatively more clearly defined than that of muscle mass (Fig. 3B). The shoulder adductors and protractors had the numerically

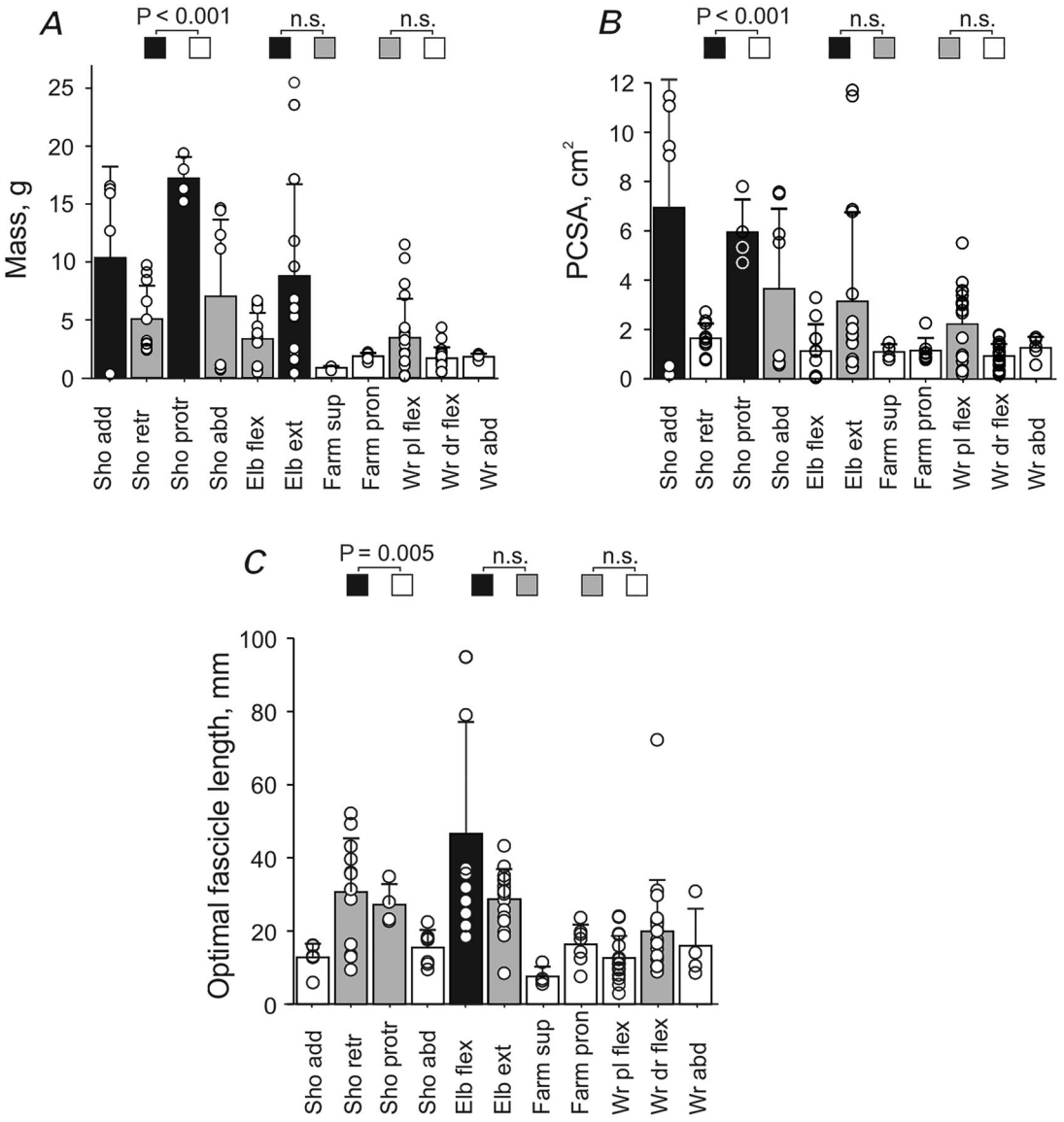

Figure 3. Morphological characteristics (mean ± SD and individual values) of 46 MTUs of the 3D forelimb model (see Fig. 1A) obtained from four specimens (Table 1, cats 2, 3, 5, 6)
A–C, mass, physiological cross-sectional area (PCSA) and optimal fascicle length, respectively, of MTU groups classified by their mechanical action in 3D. The mean values indicated by black and white bars are significantly different from each other ($P \leq 0.005$). Grey bars indicate mean values that are statistically indistinguishable from black and white bars as well as from each other. Sho, Elb, Farm, Wr indicate shoulder, elbow, forearm and wrist, respectively; add and abd, adductors and abductors; retr and protr, retractors and protractors; flex and ext, flexors and extensors; sup and pron, supinators and pronators; pl and dr, plantar and dorsi. $P \leq 0.005$ indicates significant difference, n.s. indicates no significant difference.

largest PCSAs (6.94 ± 5.20 and 5.94 ± 1.33 cm^2, respectively), roughly 3 times that of the majority of muscle groups, including shoulder retractors (1.64 ± 0.60 cm^2), forearm supinators (1.09 ± 0.31 cm^2) and pronators (1.15 ± 0.51 cm^2), wrist abductors (1.26 ± 0.45 cm^2), plantarflexors (2.21 ± 1.57 cm^2), and dorsiflexors (0.92 ± 0.49 cm^2).

The optimal fascicle length varied from 5.85 ± 2.19 mm (FDS) to 89.6 ± 9.1 mm (BCD) (Table 5), with the elbow flexor BCD being substantially longer than other muscles. The average fascicle lengths of the anti-gravity shoulder protractors and retractors were 27.2 ± 5.6 mm and 30.7 ± 14.7 mm, respectively (Fig. 3C). Fascicle lengths of elbow flexors (46.6 ± 30.5 mm) exceeded the lengths of shoulder adductors/abductors, forearm supinator/pronator and wrist plantarflexors/abductors ($P < 0.005$) but were not significantly different from elbow extensors ($P = 0.06$; 28.7 ± 8.2 mm). Fascicle length of antigravity wrist plantarflexors and their antagonists wrist dorsiflexors were not significantly different either (12.7 ± 6.0 mm *vs.* 20.0 ± 14.0 mm, $P = 0.07$). This contrasts with the hindlimb, where antigravity muscles (quadriceps, triceps surae) have substantially shorter fascicles than their counterparts (hamstrings, tibialis anterior) (Sacks & Roy, 1982).

Forelimb locomotor mechanics

Forelimb kinematic and kinetic variables obtained in all animals during overground locomotion are shown as a function of the normalized cycle time in Fig. 4 (see also Supplement 4). The mean shoulder, elbow and wrist angles (see Fig. 4A–C) showed patterns and joint angle ranges typical for cat walking (English, 1978a; Lavoie et al., 1995; Miller & Van Der Meche, 1975; Prilutsky et al., 2005). During the swing phase, shoulder and elbow angles reached their minimum values (86.8 ± 6.6° and 78.5 ± 7.3°) and the wrist its maximum value (232.7 ± 15.8°) in early to mid-swing. These instances correspond to maximal shoulder retraction, elbow flexion and wrist dorsiflexion. The maximum shoulder protraction (124.3 ± 4.5°) and elbow extension (113.5 ± 7.5°) occurred at the end of swing. During the stance phase, the shoulder retracts, while the elbow joint continues extending. The wrist joint is slightly dorsiflexing in stance before plantarflexing at end-stance.

The pattern of the forelimb length (the distance between the shoulder and the paw, Fig. 1A, sagittal view) closely resembled the elbow angle pattern with the shortest length (0.137 ± 0.009 m) in mid-swing and the peak value (0.204 ± 0.006 m) at the end of stance (Fig. 4D). The forelimb orientation changes from its maximum value (136.4 ± 2.8°) at swing onset to its minimum value (64.2 ± 5.0°) at the end of swing (Fig. 4E). The patterns of forelimb length and orientation were remarkably similar to those of the hindlimb during walking in the cat (Chang et al., 2009; Klishko et al., 2014).

The patterns and peak values of the ground reaction forces applied to the forelimb (Fig. 4F) were typical for cat walking (Farrell et al., 2014; Lavoie et al., 1995). Specifically, the vertical force peak (19.0 ± 2.6 N or 58.1 ± 8.0% body weight) occurred near the end of stance. Note that this value is approximately 20% higher than the vertical peak force of the cat hindlimb, which occurs in early stance during walking at comparable speeds (Farrell et al., 2014; Lavoie et al., 1995). The horizontal component of the ground reaction force had a negative peak in the first half of stance (−3.2 ± 1.0 N) and a positive peak in the second half (3.2 ± 0.9 N). Although the absolute values of the positive and negative peaks were the same, the area under the negative forces (force impulse) was larger, indicating that the net action of the forelimb during stance is to decelerate the body, as opposed to the hindlimbs that accelerate the body during stance (Farrell et al., 2014; Lavoie et al., 1995).

The resultant joint moments of force characterizing the action of forelimb muscles in the sagittal plane are shown in Fig. 4G–I. Wrist plantarflexors and elbow extensors produced their largest moment during stance (peak values were −0.339 ± 0.113 and −0.998 ± 0.225 N m, respectively; Fig. 4H and I). There are relatively small wrist dorsiflexion and elbow flexion moments at the end of stance and early swing, and the wrist dorsiflexors and elbow flexors continue producing flexor moments during the first half of swing, although their peak flexor moment values are very low (0.004 ± 0.002 and 0.052 ± 0.010 N m, respectively). The action of shoulder protractors located in front of the shoulder joint produced their moment of force throughout most of the stance phase with a maximum protraction moment of 1.181 ± 0.283 N m appearing closer to stance offset (Fig. 4G). The peak shoulder retraction moment (−0.305 ± 0.091 N m) occurred at stance onset. During the first third of swing, the shoulder moment is protraction (the peak of 0.023 ± 0.028 N m) before switching to retraction for the rest of swing. Patterns of wrist and elbow moments resembled corresponding ankle and knee moments of walking cats, although the magnitude of the elbow extension moment was over two times greater than the peak knee extension moment (Gregor et al., 2018; McFadyen et al., 1999). The shoulder protraction moment occurred during most of stance, as opposed to the corresponding hip flexion moment, which acts during the second half of the stance phase (Gregor et al., 2018; McFadyen et al., 1999).

The forelimb MTU lengths normalized by the optimal MTU length (see Table 5) are shown as a function of the normalized cycle time in Fig. 5A. Length changes of one-joint muscles were closely related to the joint angle patterns. The shoulder retractors located posterior to the

shoulder joint increased their length from a minimum in early swing to a peak value before swing offset. The antagonists, shoulder protractors, had opposite length changes with peak length in early swing and minimum length just before stance onset. MTU length changes of the one-joint elbow flexors followed the pattern of the elbow joint angle with minimum length in mid-swing and two local length peaks just before stance onset and stance offset. MTU length changes of one-joint elbow extensors were opposite. Patterns of MTU length changes of wrist dorsiflexors and plantarflexors were also opposite to each other with the pattern of wrist dorsiflexors demonstrating maximum length in early swing and a relatively small decrease in length during stance. The two-joint antagonists BB and TLONG likewise demonstrated opposite length changes with BB reaching a minimum MTU length in mid-swing and peak length at stance offset. The MTU length of the elbow flexors–wrist dorsiflexors similarly had a minimum in mid-swing and maximum at stance offset. The patterns of forelimb MTU length changes were generally consistent with those of cat hindlimb MTUs (Goslow et al., 1973; Gregor et al., 2006; Klishko et al., 2021). Specifically, proximal forelimb flexors (BB) and hindlimb flexors (iliopsoas, rectus femoris, sartorius medial head) located anterior to the shoulder or hip joints reach their maximum length at stance offset.

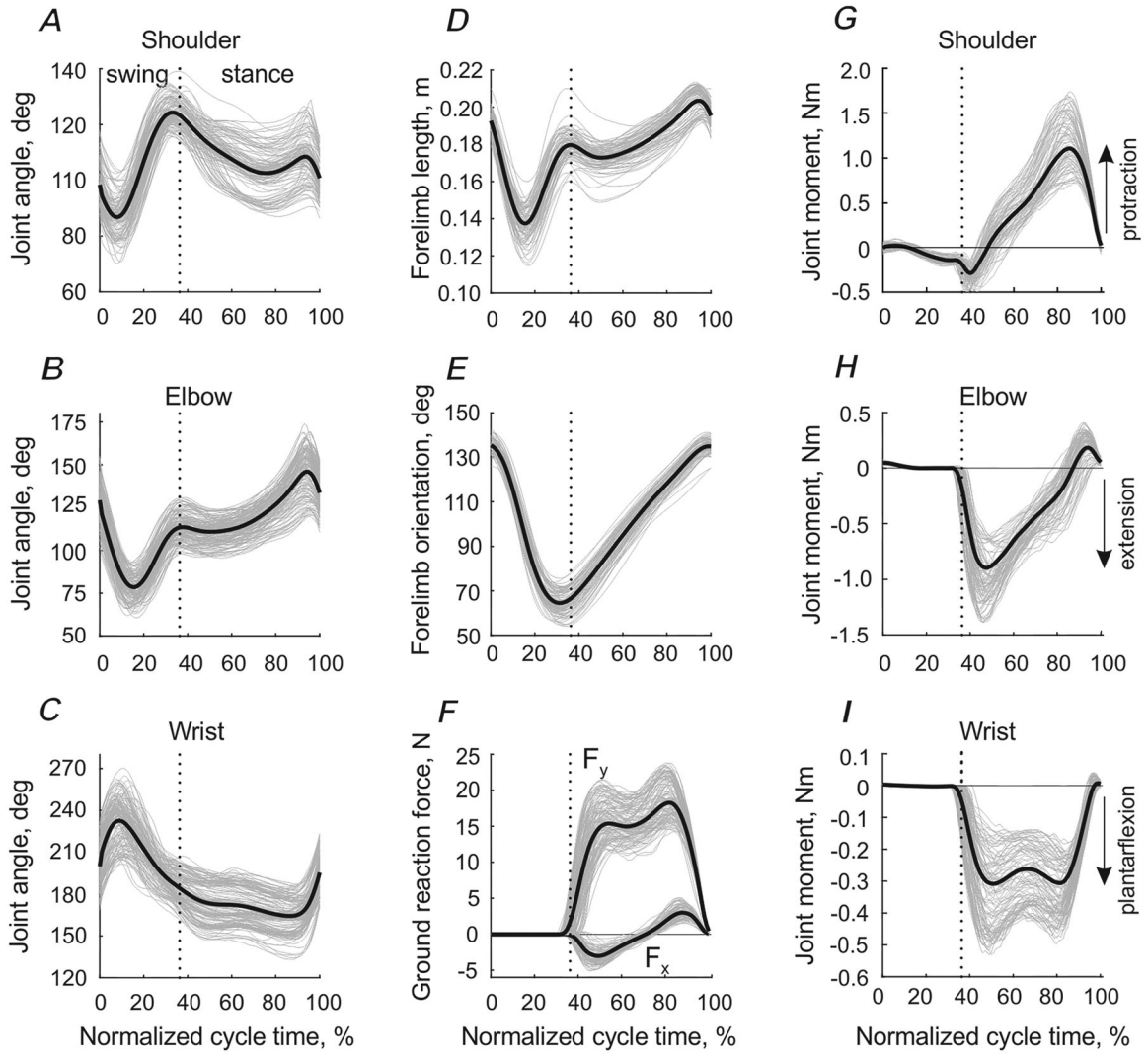

Figure 4. Forelimb mechanical variables during the cycle of overground locomotion (mean patterns are shown by thick black lines, individual cycles of different animals are shown by thin grey lines)
The mean patterns were obtained from all studied cats (n = 7) and walking cycles (n = 211) (see Table 2). *A–C*, joint angles at the shoulder, elbow and wrist, respectively. *D* and *E*, forelimb length and forelimb orientation, respectively, as defined in Fig. 1A. *F*, vertical (F_y) and horizontal (F_x) components of the ground reaction force vector. *G–I*, resultant moments of force at the shoulder, elbow and wrist joints. Vertical dotted lines separate the swing and stance phase.

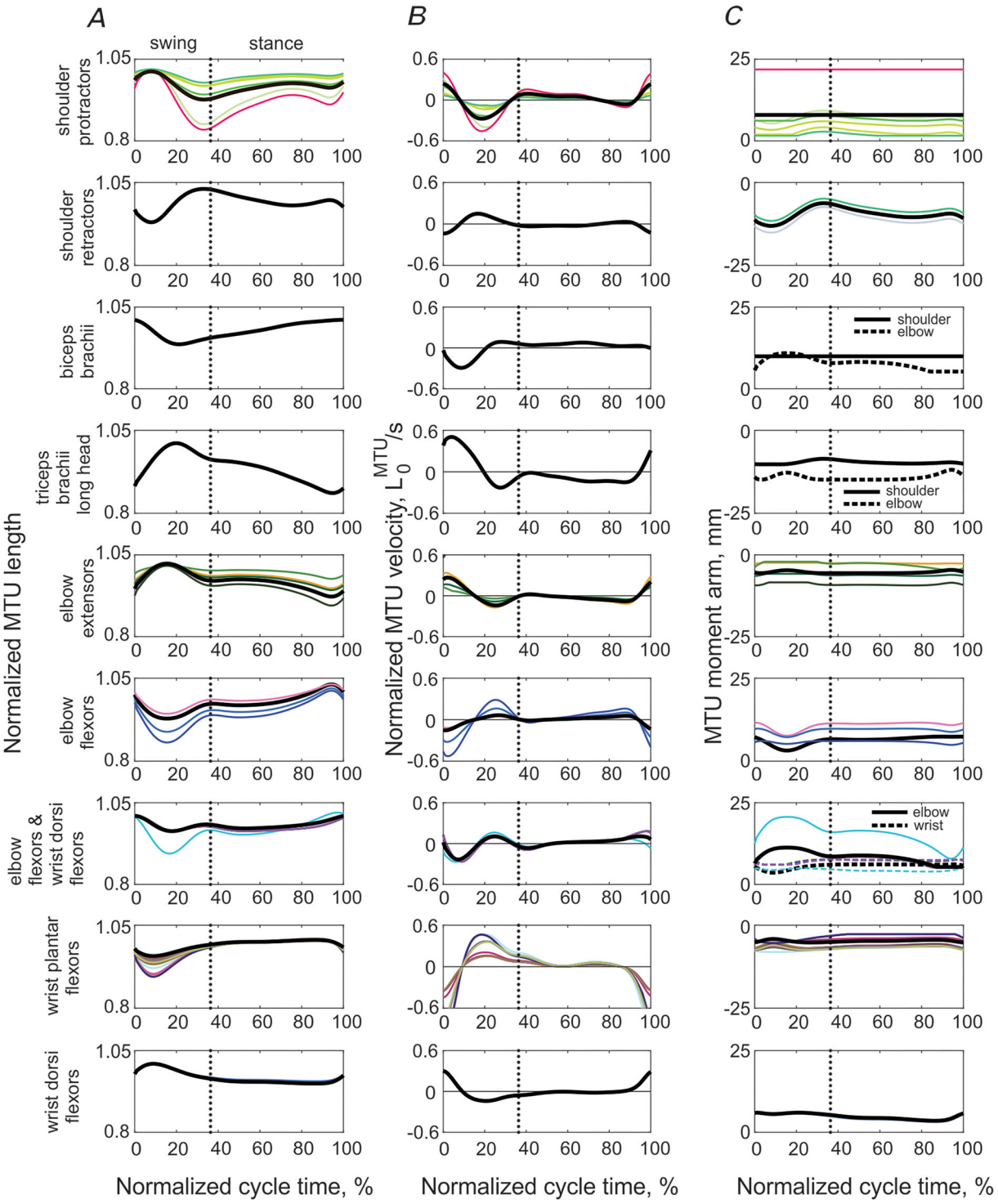

Figure 5. Computed mean normalized length (*A*), normalized velocity (*B*) and moment arms (*C*) of individual MTUs (thin coloured lines) and the equivalent MTUs representing individual MTUs with the same action at joints during the walking cycle

Colours of individual MTU patterns correspond to the colours of individual MTUs in Fig. 1A. MTU length is normalized to the optimal MTU length (L_0^{MTU}, Table 5); MTU normalized velocity units are L_0^{MTU}/s, where L_0^{MTU} is the optimal MTU length (Table 5). Positive moment arm corresponds to the direction of MTU moment of force that tends to rotate the distal link counterclockwise (see the moment sign convention in Fig. 1). The mean patterns were computed from all studied cats (n = 7) and walking cycles (n = 211) (see Table 2). [Colour figure can be viewed at wileyonlinelibrary.com]

The proximal antagonists, shoulder retractors and hip extensors reach their peak MTU lengths prior to stance onset. There were also differences in the MTU length patterns between the forelimb and hindlimb, as there is a much less pronounced stretch of the forelimb distal extensors–plantarflexors in early stance due to smaller yield at the wrist and elbow compared to the stretch of ankle plantarflexors and knee extensors.

The normalized MTU velocity changes during the walking cycle were generally similar across forelimb muscles (Fig. 5B). The greatest values of MTU shortening and lengthening velocities occurred in swing, and relatively constant velocities were seen during most of stance. Peak lengthening velocities, which are related to high activity of spindle group Ia afferents (see below), often occurred in proximal MTUs at the stance–swing transition (shoulder protractors, triceps brachii long head, one-joint elbow extensors) and in distal wrist dorsiflexors.

The forelimb moment arms changed relatively little during the walking cycle for most MTUs, except for shoulder retractors (range: 7.4–15.1 mm for TJ and 4.9–11.5 mm for SD) and ECR (range: 7.9–20.7 mm) (Fig. 5C). The absolute value of the moment arm at a joint determines the range of MTU length change and peak MTU velocity (e.g. compare the moment arms, lengths and velocity peaks among the shoulder protractors or elbow extensors; Fig. 5). As evident from Fig. 5C, moment arm values of proximal MTUs, such as shoulder protractors and retractors, BB, and TLONG, were substantially longer than those of distal MTUs of wrist dorsiflexors and plantarflexors.

Maximum moments of individual and equivalent MTUs during locomotion

The *k*-means clustering algorithm applied to the mean peaks of maximum moments of force produced by 40 MTUs during walking of all cats revealed nine clusters or MTU groups with unique muscle actions at forelimb joints in the sagittal plane (Fig. 1B). These included shoulder protractors (6 MTUs), shoulder retractors (2 MTUs), shoulder protractor–elbow flexor (1 MTU), shoulder retractor–elbow extensor (1 MTU), elbow extensors (4 MTUs), elbow flexors (3 MTUs), elbow flexors–wrist dorsiflexors (5 MTUs), wrist plantarflexors (16 MTUs) and wrist dorsiflexors (2 MTUs). Because synergistic muscles are normally activated together (Buchanan et al., 1986; Hug et al., 2022; Prilutsky, 2000a,b), it is possible to simplify the forelimb musculoskeletal model by replacing the action of individual MTUs in each cluster group by an equivalent MTU with a similar muscle action. The morphological and geometric parameters of such equivalent muscles were obtained as described in 'Methods' and are listed in Table 5 (bold font) and Table 7. The comparison of the sum of the maximum moments of each cluster with the corresponding moment of the equivalent MTU, computed assuming maximum activation of the MTUs, $A = 1$ (see eqns (2)–(6)), demonstrated a close match (Fig. 6A–I). The normalized maximum difference did not exceed 7% for all MTU clusters except for one (elbow flexors, 11%).

The maximum potential for moment production occurred in the antigravity muscle groups (shoulder protractors, elbow extensors and wrist plantarflexors) during stance or at the stance–swing transition. Their antagonists demonstrated peak maximum moments during swing (shoulder retractors, shoulder retractor–elbow extensor TLONG and wrist dorsiflexors). The two-joint MTUs contributed greater maximum moments of force during stance to the joints in which these MTUs produce an extension action, such as shoulder protraction for BB (Fig. 6C) and elbow extension for TLONG (Fig. 6D). The elbow flexors–wrist dorsiflexors produced substantially greater peaks of maximum moment for elbow flexion during the second half of swing and the middle portion of stance (Fig. 6G).

The resultant moments of force during walking determined by inverse dynamics analysis were substantially lower in magnitude than the maximum possible moments, except for elbow and wrist dorsiflexion moments (Fig. 6K–M). The greatest unused moment potential occurred in wrist plantarflexors, which could be related to the additional functions of the forelimb, including hunting and defense.

Motor output of forelimb MTUs during walking

We computed activation of each MTU during the walking cycle by minimizing the cost function of minimum fatigue (eqn (16)) under the constraints of muscle contractile force–length–velocity properties (eqns (2)–(6)), resultant joint moments of force during walking (eqn (17)), and minimum and maximum activations (eqn (18)). Antigravity individual MTUs and equivalent MTUs representing the functional groups revealed by the cluster analysis were activated primarily during the stance phase (Fig. 7A; shoulder protractors, elbow extensors, wrist plantarflexors). Their antagonists (shoulder retractors, elbow flexors, two-joint elbow flexors–wrist dorsiflexors, but not one-joint wrist dorsiflexors) were mostly active during swing. The two-joint shoulder protractor–elbow flexor BB was active at end stance and early swing, whereas the two-joint shoulder retractor–elbow extensor TLONG was active from end swing and throughout most of stance. No activation was predicted for one-joint wrist dorsiflexors (Fig. 7A), although the resultant wrist dorsiflexion moment of force was flexor in early swing and late stance (Fig 4I). All synergistic MTUs

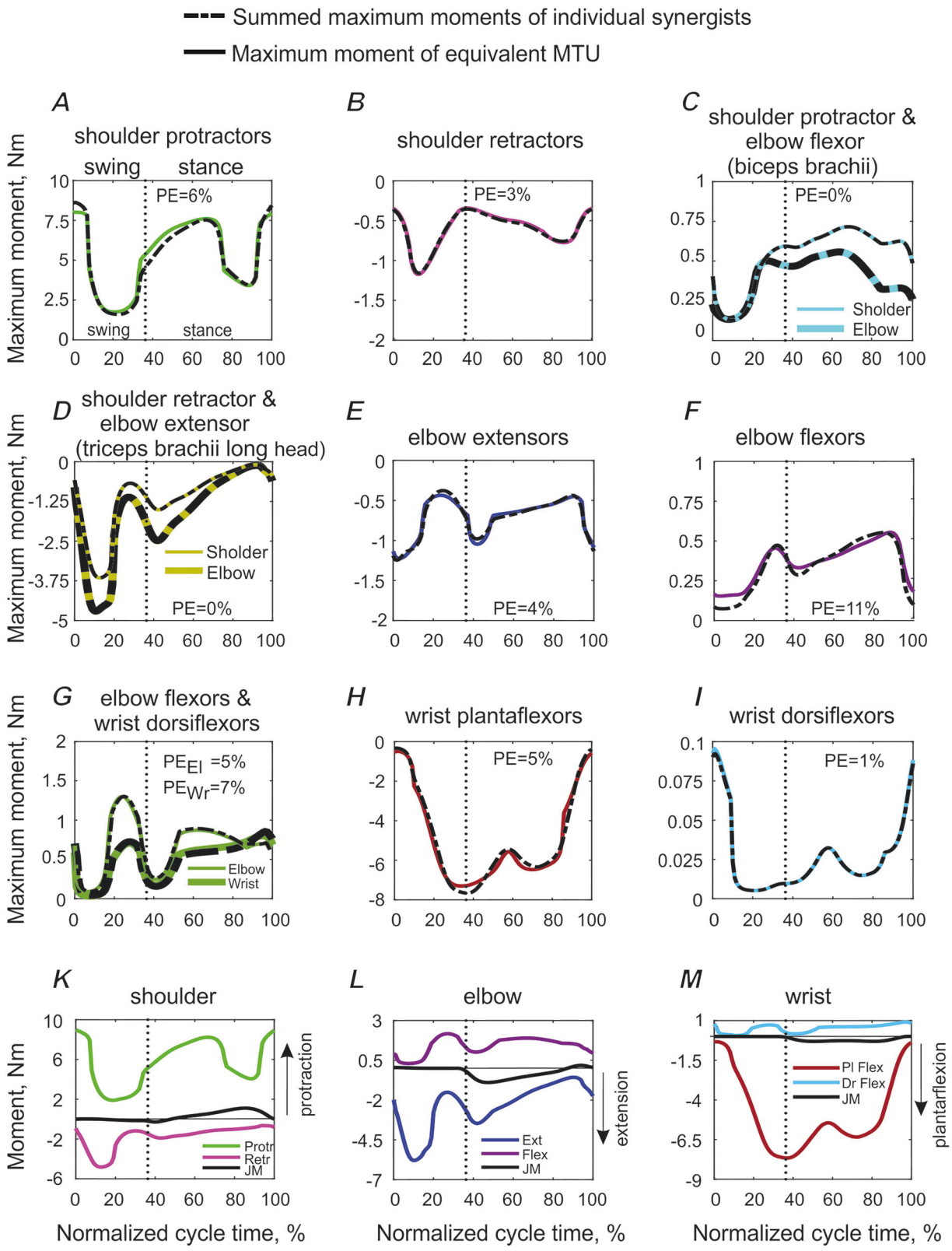

Figure 6. Mean maximum moments of force and mean resultant moments of force at forelimb joints during the walking cycle
The vertical dotted lines separate the swing and stance phase. The moment sign convention is the same as in Fig. 1A, that is, positive direction corresponds to the counterclockwise rotation of the distal segment at the joint. The mean patterns were computed from all studied cats (n = 7) and walking cycles (n = 211) (see Table 2). *A–I*,

comparisons of the summed maximum moment of force produced by individual synergists at joints (black dashed lines) and by the equivalent MTU with the same mechanical action at the joints (continuous coloured lines). Colours of moments produced by the equivalent MTUs correspond to the colours of equivalent muscles in Fig. 1B. Two-joint MTUs (biceps brachii, triceps brachii long head and elbow flexors–wrist dorsiflexors) produce maximal moments at each joint they span. PE is the percentage error between the sum of maximum moments produced by synergists at the joints and by their equivalent muscle. *K–M*, comparisons of the maximum moments of force produced by all equivalent MTUs in both directions with the actual mean moment of force (see Fig. 4G–I) during the walking cycle. Protr and Rets, protraction and retraction; Ext and Flex, extension and flexion; Pl and Dr, plantar and dorsi. [Colour figure can be viewed at wileyonlinelibrary.com]

within each functional group were activated with generally similar patterns, except for pronator teres (PT) among elbow flexors. In 3D, PT is primarily a pronator and has extremely short fascicles, relative to other elbow flexors. The computed activations of the one-joint antagonists (shoulder protractors–retractors and elbow extensors–flexors) demonstrated reciprocal activation. Two-joint muscles often had peak activation when the moments produced by these muscles at both joints coincided with the direction of the resultant joint moments. For example, BB had two activity bursts, in early swing and late stance (Fig. 7A), when there was simultaneous production of resultant shoulder protraction moment (Fig. 4G) and resultant elbow flexion moment (Fig. 4H). The TLONG initiated its activity burst earlier than the one-joint elbow extensors (in late swing and swing–stance transition; Fig. 7A) when there was a combination of shoulder retraction (Fig. 4G) and elbow extension resultant moments (Fig. 4H). Two of the three activation peaks of two-joint elbow flexors–wrist dorsiflexors at the end of stance and early swing transition (Fig. 7A) coincided with the simultaneous production of a resultant flexion moment at the elbow (Fig. 4H) and a dorsiflexion moment at the wrist (Fig. 4I).

The computed activation when compared with the recorded EMG activity of selected muscles showed that such minimum fatigue minimization generally predicted the reciprocal activation of antagonist forelimb muscles, such as TLAT *vs*. PT and BR, and BB *vs*. TLONG, as well as synergistic activation of agonists, such as TLONG with TLAT and PT with BR (Fig. 8). Computed activations using the models with 40 MTUs and nine equivalent MTUs were generally similar except for PT where the 40-MTU model demonstrated a closer match with the recorded EMG activity (Fig. 8). Both models showed that the computed activity patterns of SPS and both heads of triceps brachii were qualitatively similar to EMG activity (Fig. 8). For the other muscles, the computed activations by the two models showed some discrepancies with EMG activity (Fig. 8).

Computed MTU forces generally had similar patterns to the computed activations with some minor exceptions (Fig. 7B). This is expected given that MTU force also depends on MTU length and velocity of length change (see eqns (2)–(6)). This also explains the difference in the magnitudes of the activation and forces for individual MTUs within functional groups (e.g. shoulder protractors and retractors). The computed forces of the functional groups were much larger for proximal antigravity muscles, shoulder protractors and TLONG, with peak forces approaching 60 N. The peak forces of other MTUs did not exceed 10 N.

Patterns of the moments of force of individual and equivalent MTUs resembled the force patterns of the same MTUs (Fig. 7C), indicating relatively small changes in the MTU moment arms during the walking cycle. The moments produced by the two-joint muscles at the joints they span had different magnitudes; protraction shoulder moment of BB was greater than flexion elbow moment, elbow extension moment of TLONG exceeded shoulder retraction moment, and elbow flexion moments of elbow flexors–wrist dorsiflexors were greater than wrist dorsiflexion moments.

Computed proprioceptive activity of forelimb MTUs

The developed forelimb musculoskeletal model allowed computing the activity of muscle spindle group Ia and II afferents using the calculated velocity, length (Fig. 5A and B), and activation (Fig. 7A) of individual MTUs (eqns (7) and (8)), as well as the activity of Golgi tendon organ group Ib afferents using the calculated MTU forces (Fig. 7B; eqn (9)). Activity patterns of Ia afferents (Fig. 9A) resembled patterns of MTU velocities. Specifically, one-joint shoulder protractors, two-joint TLONG, one-joint elbow extensors and one-joint wrist dorsiflexors reached their peak Ia activity at the stance–swing transition, which corresponded to the peak velocities of these MTUs (Fig. 5B). One-joint shoulder retractors, two-joint BB, one-joint elbow flexors and wrist plantarflexors reached their peak Ia activity between the middle and the end of swing.

The muscle spindle group II activity closely matched length changes of the corresponding MTUs (Figs 5A and 9B). MTUs located anteriorly to the forelimb joints (one-joint shoulder protractors, two-joint BB, one-joint elbow flexors and two-joint elbow flexors–wrist dorsiflexors) reached their maximum length and spindle group II activity near the stance–swing transition. One-joint shoulder retractors and wrist plantarflexors reached their maximum length and spindle group II activity at the swing–stance transition. The magnitude of

MTU length- and velocity-dependent afferent activities of individual MTUs increased with the MTU moment arm, the distance between the line of MTU action and the joint centre. For example, the shoulder protractor SPS (pink trace in Figs 1A and 9A, B) was farthest from the shoulder centre and demonstrated the highest rates of spindle activity. This is because MTU length change due to joint angle changes is proportional to the MTU moment arm (An et al., 1983).

Because the firing rate of Ib afferents is proportional to muscle force (see eqn (9)), the patterns of MTU muscle forces and group Ib afferent activities were identical

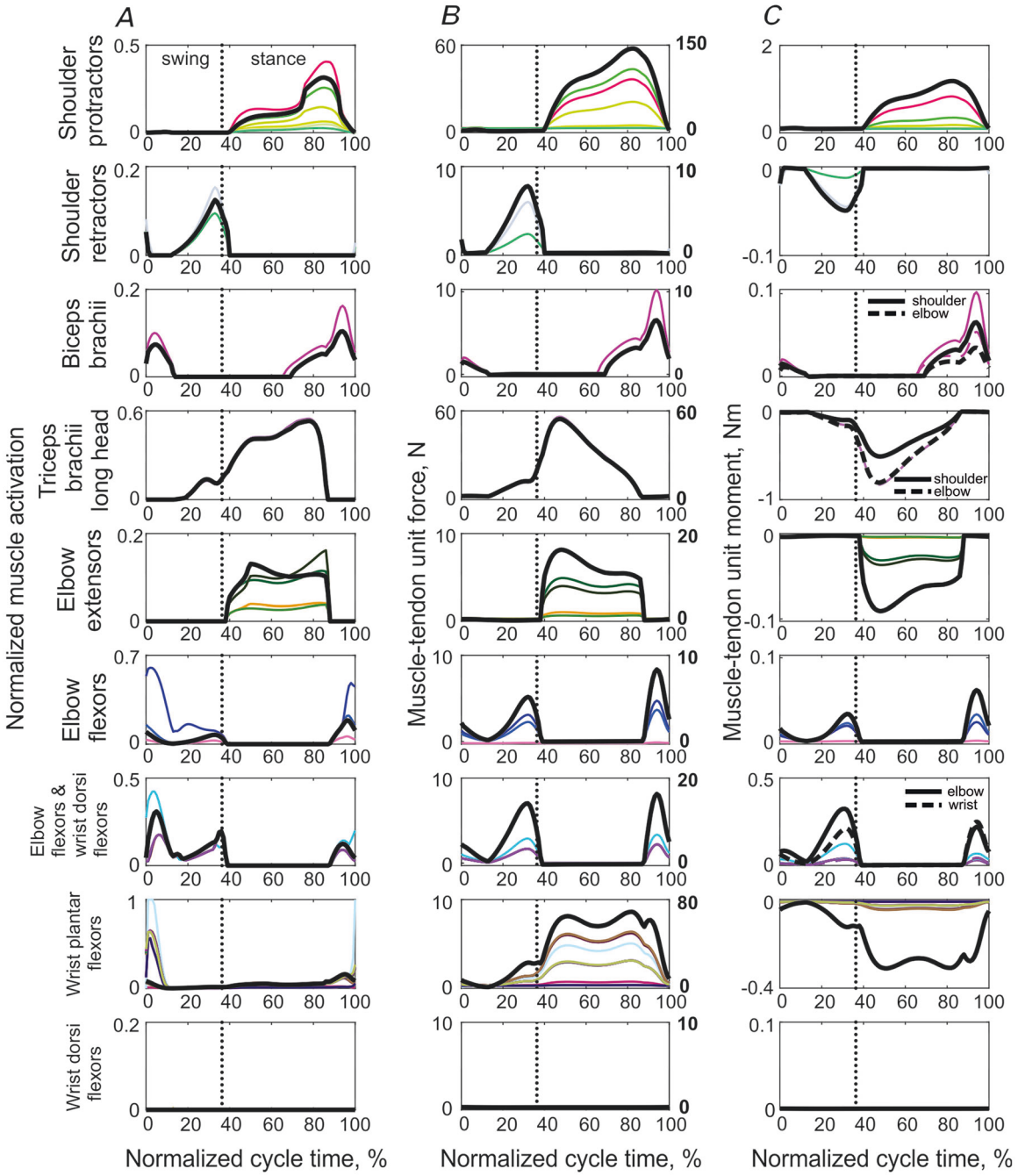

Figure 7. Mean computed activation (*A*), force (*B*) and moment of force (*C*) of individual MTUs (thin coloured lines) and the equivalent MTUs (thick black lines) during the walking cycle
Two-joint MTUs produce moments of force at each joint they span. The vertical dotted lines separate the swing and stance phase. The moment sign convention is the same as in Fig. 1A. Colours of individual MTU patterns correspond to the colours of individual MTUs in Fig. 1A. The mean patterns were computed from all studied cats ($n = 7$) and walking cycles ($n = 211$) (see Table 2). [Colour figure can be viewed at wileyonlinelibrary.com]

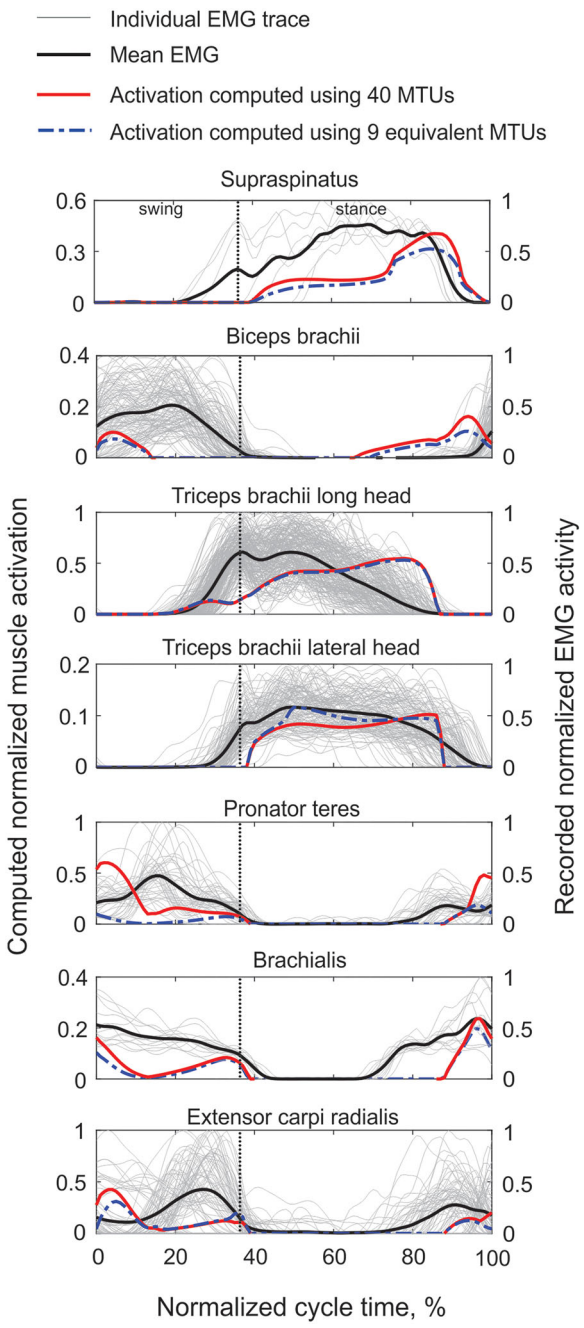

Figure 8. Comparison of mean patterns of computed activation of selected MTUs with the recorded EMG activity
The vertical dotted lines separate the swing and stance phase. The computed activation has the range from 0 to 1. The recorded EMG patterns were normalized by the peak value across all cycles within each animal. The computed mean activation patterns were obtained from all studied cats ($n = 7$) and walking cycles ($n = 211$) (see Table 2). Red lines show activations computed using the full forelimb musculoskeletal model with 40 MTUs; blue lines show activations computed using a reduced forelimb model with nine equivalent muscles (see eqns (16)–(18) and Fig. 1B). The mean patterns of recorded EMG (thick black lines) are averages of 531 cycles (thin grey lines) of 16 cats (Table 4). [Colour figure can be viewed at wileyonlinelibrary.com]

(Figs 7B and 9C). Thus, antigravity forelimb muscle group Ib afferents were active during stance, while Ib afferent activity of their antagonists occurred during the swing phase.

The peak rates of computed proprioceptive activity did not exceed 200 Hz, which is consistent with the rates of proprioceptive afferents of hindlimb muscles during cat locomotion (Loeb & Duysens, 1979; Prochazka & Gorassini, 1998). Our computed rates were also consistent with rates of group Ia afferents of selected shoulder protractors and retractors and elbow flexors and extensors maintained at a constant length while the other three limbs of the cat decerebrate preparation performed treadmill locomotion (Cabelguen et al., 1984).

We used the computed activation and proprioceptive activity of 40 MTUs during walking, the known distribution of motoneuron pools of selected cat forelimb muscles in cervical segments (Table 8) (Fritz, Illert, Reeh, 1986; Fritz, Illert, Saggau, 1986; Horner & Kummel, 1993), and assumed the same rostro-caudal distribution of motoneuron pools and their proprioceptive inputs in the cervical spinal cord (Levine et al., 2012; Sterling & Kuypers, 1967a,b) to compute spatiotemporal maps of motor and sensory activity in cervical spinal segments during the walking cycle (Fig. 10).

According to Table 8, segment C5 contains a relatively small proportion of motoneurons (1–9%) of one-joint shoulder protractors, two-joint elbow flexors–wrist dorsiflexors (9%) and one-joint wrist dorsiflexors (3%). Motoneurons of the two-joint BB constituted a substantial proportion of the total at C5 (37%). Segments C6 and C7 contained the largest proportions of motoneurons innervating mostly proximal muscles: the one-joint shoulder protractors (between 20% and 87% for most MTUs), one-joint retractors (33–67% for SD, 1–99% for TJ), the two-joint BB (19–40%), one-joint elbow flexors (1–94%) and the two-joint elbow flexor–wrist dorsiflexor ECR (32–59%). Segments C8 and T1 contained the largest proportion of motoneurons of the two-joint elbow flexor–wrist dorsiflexor EDC (63% and 36%) and one-joint wrist plantarflexors (28–72%). Since we could not find the distribution of motoneurons in the two-joint MTUs spanning the shoulder and elbow (BB and TLONG) and one-joint elbow extensors, we took these data from the corresponding MTUs of monkey (Jenny & Inukai, 1983). Most BB motoneurons in the monkey's spinal cord are located in segments C5–C7 (19–37%), while TLONG and elbow extensors are in segments C7–T1 (22–52%). In that monkey study, the authors compared the distribution of motoneurons of the EDC between four monkeys and three cats and found that the total number of motoneurons was 295.0 ± 30.2 and 299.0 ± 19.2, respectively, and all of them were in segments C7, C8 and T1. The distribution of motoneurons for these segments was 1.1 ± 1.0%, 55.0 ± 7.2% and 43.9 ± 7.9% for the monkeys and 2.3 ± 2.1%,

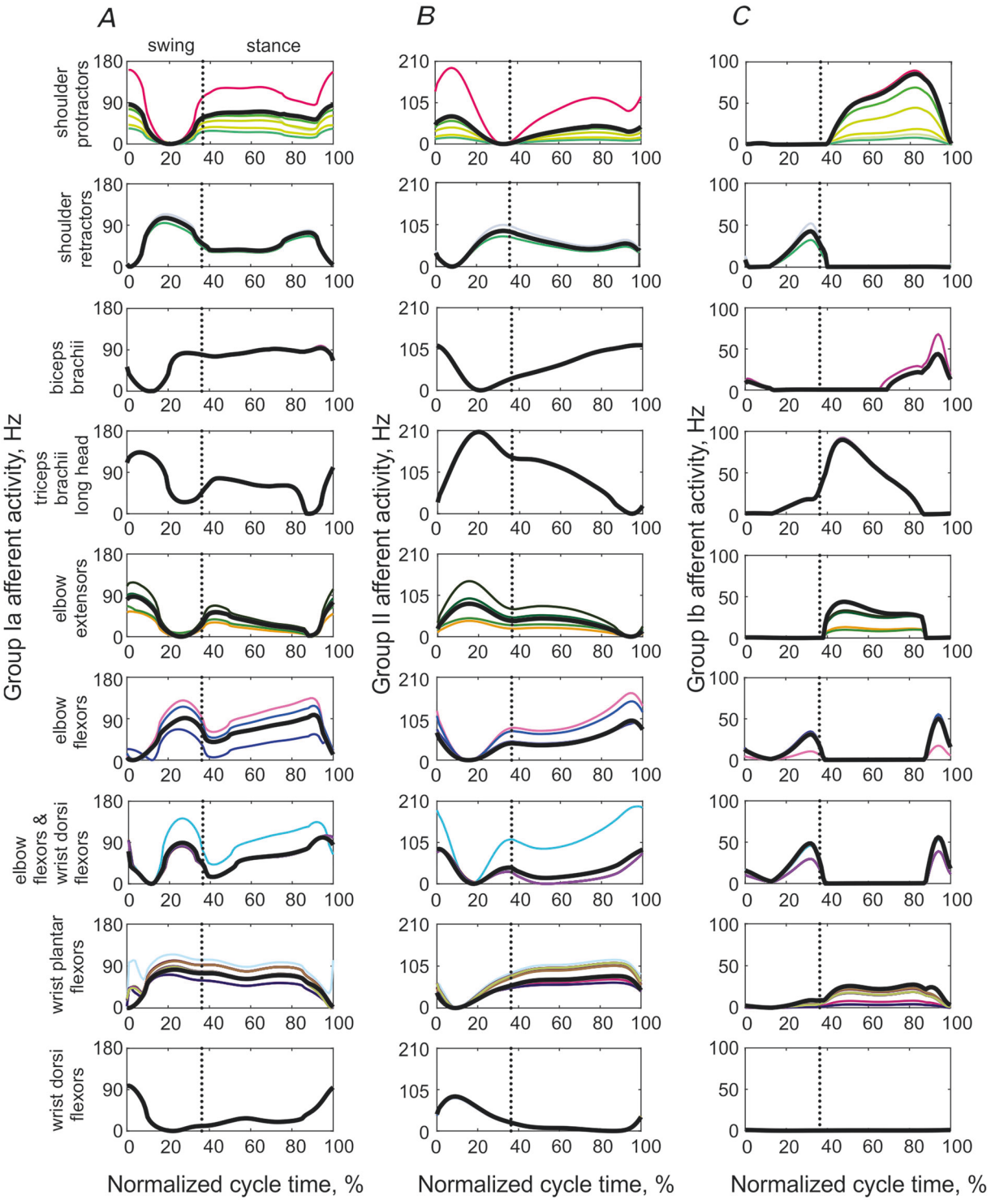

Figure 9. Mean computed activity of muscle spindle group Ia afferents (*A*), muscle spindle group II afferents (*B*) and Golgi tendon group Ib afferents (*C*) of individual MTUs (thin coloured lines) and of the equivalent MTUs (thick black lines) during the walking cycle
The vertical dotted lines separate the swing and stance phase. Colours of individual MTU patterns correspond to the colours of individual MTUs in Fig. 1A. The mean patterns were computed from all studied cats (n = 7) and walking cycles (n = 211) (see Table 2). [Colour figure can be viewed at wileyonlinelibrary.com]

75.8 ± 20.6% and 21.3–23.6% for the cats, respectively. The mean motoneuron distributions of EDC from Jenny & Inukai (1983) were within 1 standard deviation of both the monkey EDC and the cat EDC data of Fritz, Illert, Saggau (1986). Thus, replacing the missing cat data for the three MTU groups in Table 8 with data from the monkey is reasonable.

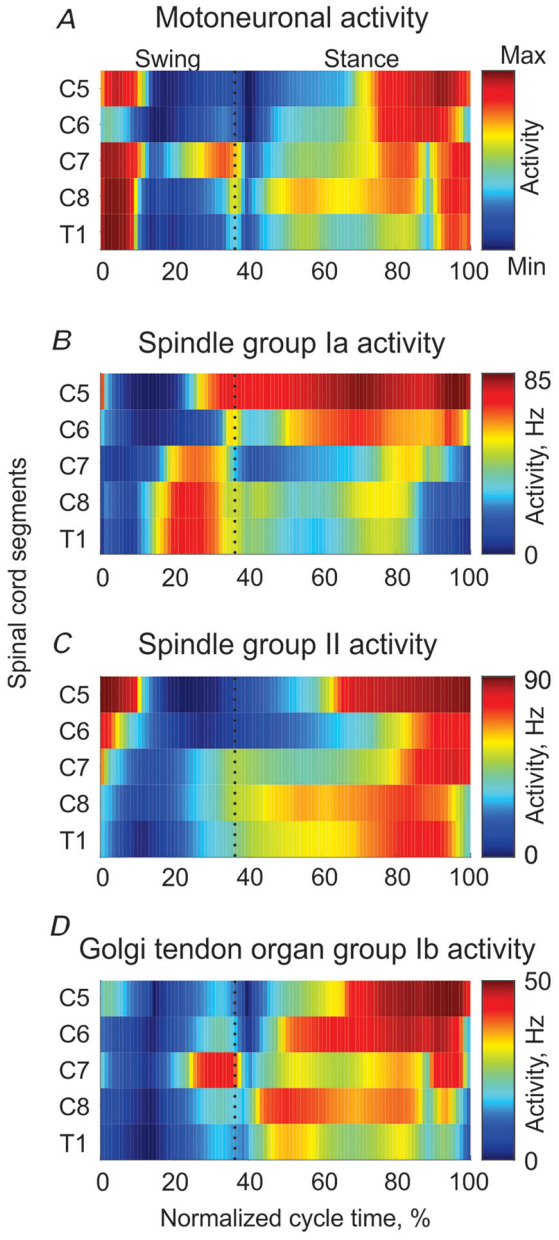

Figure 10. Spatiotemporal maps of computed motoneuronal activation (*A*), afferent activity of spindle group Ia (*B*), spindle group II (*C*) and Golgi tendon organ group Ib (*D*) afferents projected to the corresponding cervical spinal segments during the walking cycle (see text and eqns (7)–(9) and (19) for details)
The vertical dotted lines separate the swing and stance phase. The spatiotemporal maps were computed from all studied cats ($n = 7$) and walking cycles ($n = 211$) (see Table 2). [Colour figure can be viewed at wileyonlinelibrary.com]

The computed spatiotemporal maps of normalized motoneuronal activity shown in Fig. 10A indicate the total proportion of motoneurons recruited in segments C5–T1 during the overground walking cycle. Thus, MTUs with high normalized activity during walking, like some one-joint wrist plantarflexors and elbow flexors in early swing (Fig. 7A), had the greatest contribution to the spatiotemporal map. The normalized motoneuronal activity was high during the stance phase, the stance–swing transition and early swing, and it was distributed across segments C5 through T1 (Fig. 10A). An elevated activity in the stance phase started at the swing–stance transition and occurred mostly in segments C7 and C8 because of muscles involved in shoulder retraction with simultaneous elbow extension and simultaneous elbow flexion and wrist dorsiflexion (see also Fig. 7A and Table 8). The stance-related activity of motoneurons shifts from caudal segments C7–T1 in early to mid-stance to segments C5–C7 in the second part of stance from ∼70% to 90% of the cycle. The highest proportion of active motoneurons during late stance occurred in rostral segments C5 and C6. This activity reflected recruitment of shoulder protractors and two-joint biceps brachii. Motoneurons of elbow extensors and wrist plantarflexors, which are mostly located in more caudal cervical segments, were also recruited during late stance but to a lower degree. At end stance (90–100% of the cycle) and early swing (0–10%), relatively high motoneuronal activity occurred in segments C5–T1 that was related to recruitment of the two-joint shoulder protractor–elbow flexor BB and elbow flexors–wrist dorsiflexors (ECR, EDC), as well as one-joint elbow flexors and wrist plantarflexors (Fig. 7A). During most of the swing phase, shoulder retractors, elbow flexors and wrist dorsiflexors were active, but a relatively small proportion of their motoneurons was recruited across segments C5–T1 (Fig. 10A).

The spatiotemporal map of spindle group Ia afferent activity that serves as sensory input to the motoneurons in the corresponding spinal segments is shown in Fig. 10B. Group Ia activity started increasing from its minimum level at mid-swing. This activity was initiated at caudal segments T1 and C8 (afferents of one-joint wrist plantarflexors and two-joint elbow flexor–wrist dorsiflexor EDC; Fig. 9A) and continued rostrally to segments C7 (two-joint elbow flexor–wrist dorsiflexor ECR, one-joint elbow flexors, two-joint elbow flexor–shoulder protractor BB, one-joint shoulder retractors) and C5 (BB). During the stance phase, the greatest Ia activity occurred in segments C6 and C5 (afferents of one-joint shoulder protractors and elbow flexors, two-joint BB and ECR).

The spatiotemporal map of spindle group II afferent activity started increasing at end swing and the swing–stance transition, especially in segments C7 and C8, associated with increasing length of one-joint shoulder retractors, elbow flexors and wrist plantarflexors, as well as two-joint elbow flexors–wrist dorsiflexors (Figs 9B and 10C). This activity became progressively greater during stance in segments T1 and C8 (wrist plantarflexors and two-joint EDC) and C5 (two-joint BB). The peak of group II afferent activity occurred at the stance–swing transition in segments C5–C7. This activity corresponded to recruitment of group II afferents of two-joint BB and ECR and one-joint elbow flexors and shoulder protractors (Figs 9B and 10C).

The spatiotemporal map of group Ib afferent activity was similar to the map of motoneuronal activity. All segments from C5 to T1 had higher activity during stance and this activity was associated with one-joint shoulder protractors, elbow extensors and wrist plantarflexors, as well as two-joint BB (Fig. 10D). One noticeable difference between the spatiotemporal maps of motoneuron and Ib activation was the lack of high Ib activity in early swing because of low force production by wrist plantarflexors and elbow flexors despite their relatively high computed motoneuronal recruitment.

Discussion

The goal of this study was to determine morphological characteristics of the cat's forelimb muscles and evaluate their contributions to kinetics of locomotion and motion-dependent sensory feedback. We addressed this goal by measuring forelimb morphological characteristics *post mortem* and by recording forelimb kinematics, ground reaction forces and EMG activity of selected muscles during walking. We also used the computed length, velocity, activation and force of each forelimb MTU during walking to estimate the motion-dependent sensory activity of muscle proprioceptors. Such comprehensive information allows us to analyse the role of forelimb morphology in mammalian locomotor with the level of detail unavailable previously.

Before discussing potential contributions of forelimb morphology to motor output and sensory feedback during locomotion, we consider the effects of potential errors in determining morphological characteristics on computed variables and discuss study limitations.

Effects of model sensitivity to model parameter changes

As discussed in 'Methods', the computed motor outputs and proprioceptive signals of the forelimb model depend on multiple model parameters, including optimal MTU length, maximal muscle shortening velocity, PCSA, pennation angle (see eqns (1)–(6), Table 5), and geometric parameters describing the MTU path with respect to the joints (Fig. 2 and Table 7). To evaluate sensitivity of the computed maximum moments of each equivalent MTU averaged over the walking cycle to changes in major morphological and geometric MTU parameters, we computed the first-order global sensitivity index for each parameter based on the Sobol method (Sobol, 2001) implemented in the Global Sensitivity Analysis Toolbox (flax, 2022). The first-order indices (main effects) measure the contribution of each model parameter to the total output variance (the variance of the mean maximum moment in our case), neglecting interaction effects among the parameters; the first-order index has a range of 0 to 1 (Qian & Mahdi, 2020). The effects of random changes in each parameter within 10% of its nominal value from Tables 5 and 7 on the computed first-order sensitivity indices are shown in Fig. 11. The maximum moment is most sensitive to changes in PCSA for all muscle groups, followed by geometric parameters defining the locations of the MTU origin and insertion that in turn define the MTU moment arms. The optimal muscle fascicle length affects the variance of the maximum moment of the two-joint shoulder retractors–elbow extensors, wrist dorsiflexors and shoulder protractors, although to a lesser extent. The normalized maximum muscle shortening velocity, percentage of slow-twitch fibres and pennation angle do not have noticeable effects on the maximum moment variance. Previous musculoskeletal modelling studies likewise found that the resultant moment of force at the joint and related mechanical variables are most sensitive to changes in PCSA and muscle moment arms (Raikova & Prilutsky, 2001; Ramalingasetty et al., 2021). The PCSA can be accurately obtained *post mortem* using eqn (1). The situation is more complex for determining accurate locations of the MTU origin and insertion sites because of their broad and complex 3D areas in most muscles. The moment arm value is also affected by the accuracy of determining the joint rotation axis or centre. One way to improve the accuracy of determining the MTU moment arm is to use the tendon-excursion method (An et al., 1983), which does not require the muscle attachment points and the joint centre of rotation. If coordinates of MTU attachment points are required to compute MTU length and velocity during movement, the accuracy determining these and other parameters can be improved by adjusting the measured parameters by minimizing the difference between the recorded and simulated movement mechanics and muscle activity (Bunderson et al., 2012; Neptune et al., 2008; Prilutsky et al., 2016).

Study limitations

Because we could not directly measure the motor output and proprioceptive signals of forelimb muscles, we used a modelling approach and simplifying assumptions to evaluate sensorimotor functions of these muscles in locomotion. We determined MTU activations during walking by minimizing the function of muscle fatigue (Crowninshield & Brand, 1981). This and similar optimization criteria minimizing the sense of fatigue and effort, metabolic energy expenditure and movement variability have demonstrated reasonable performance predicting recorded muscle activations or muscle forces during human and cat locomotion and other skilled/reflex motor behaviours (Anderson & Pandy, 2001; Crowninshield & Brand, 1981; Haruno & Wolpert, 2005; Prilutsky, 2000a,b; Prilutsky et al., 1997). Comparing the activation patterns of seven forelimb muscles computed from the 40-MTU model with the corresponding EMG recordings during walking in this study, we can see that only five MTUs demonstrate some qualitative agreement (Fig. 8; SPS, TLAT, TLONG, PT, BR). Note that we cannot compare the magnitudes of the computed and recorded activity (the EMG magnitude is arbitrary). We also need to account for the muscle activation and deactivation times that are ignored in our static optimization; this partially explains the earlier EMG onset and offset compared to computed activations in some MTUs (e.g. SPS, TLAT, TLONG, PT, BR) but are accounted for in dynamic optimization (Anderson & Pandy, 2001; Neptune et al., 2008; Prilutsky et al., 2016). The earlier appearance of muscle EMG compared to MTU force production depends on the electromechanical delay caused in part by developing tendon tension, which is muscle- and task-dependent. Muscles with shorter tendons undergoing lengthening actions tend to have shorter electromechanical delays (Komi, 2003). In general, computed

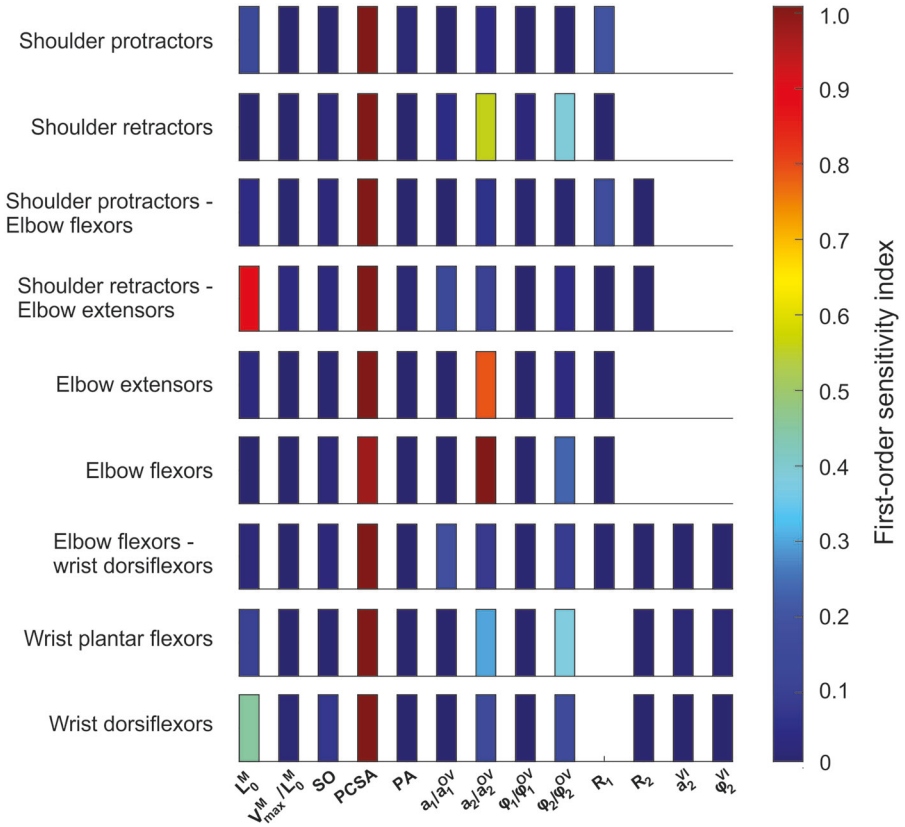

Figure 11. Sensitivity of the computed maximum moment of force averaged over the walking cycle for each equivalent MTU to major morphological and geometric model parameters
L_0^M, optimal muscle fascicle length; V_{max}^M/L_0^M, normalized maximum fascicle shortening velocity; SO, percentage of slow-twitch muscle fibres; PCSA, physiological cross-sectional area; PA, pennation angle; a_1 and φ_1, parameters defining the origin of MTU (see Fig. 2 and Table 7); a_1^{OV} and φ_1^{OV}, parameters defining the origin of MTU path between the origin and the via point; a_2 and φ_2, parameters defining the insertion of MTU; a_2^{OV} and φ_2^{OV}, parameters defining the insertion of MTU path between the origin and the via point; a_2^{VI} and φ_2^{VI}, parameters defining the insertion of MTU path between the via point and insertion; R_1 and R_2, radii of joints spanned by a two-joint MTU. The maximal moments of force were computed from all studied cats ($n = 7$) and walking cycles ($n = 211$) (see Table 2). [Colour figure can be viewed at wileyonlinelibrary.com]

forelimb activations less accurately matched recorded muscle activity or force compared to the cat hindlimb (Prilutsky et al., 1997) or human leg muscles (Anderson & Pandy, 2001; Crowninshield & Brand, 1981). This can be explained by several factors, including a more complex organization of forelimb/arm muscle morphology, with a greater number of muscle compartments with separate innervations and different activity during a single motor task (Brown et al., 2007; English & Weeks, 1987). Thus, our computed MTU activations should be considered with caution. Nevertheless, the main activity bursts of major extensor and flexor MTUs were reproduced by computed activations of the 40-MTU model (SPS, TLAT, TLONG, PT, BR) with only partial reproduction of EMG patterns of two-joint muscles (BB, ECR) (Fig. 8).

We also assumed that the proportion of proprioceptive axons entering a spinal cord segment from a given MTU corresponds to the proportion of motoneurons of this MTU in the same segment. Although, in general, somatotopy between muscle motoneurons and corresponding muscle afferents has been established (Fritz, Illert, Reeh, 1986; Fritz, Illert, Saggau, 1986; Levine et al., 2012; Sterling & Kuypers, 1967a,b), we do not know if proportions of motoneurons and proprioceptive afferents entering the same spinal segments are the same. We found only one study in two monkeys in which the number of motoneurons and dorsal root ganglion neurons labelled by the retrograde transport of horseradish peroxidase from the same muscle (EDC) were determined in segments C5–T2 and showed only rough qualitative agreement (Jenny & Inukai, 1983).

We analysed muscle mechanical actions only in the sagittal plane mainly because we were limited by motion capture of two markers on each forelimb segment and lack of information on the moment of inertia and centre of mass location of cat forelimb segments in the orthogonal planes. Although we could circumvent these limitations by attaching additional markers to each body segment (Andrada et al., 2017; Brown et al., 2018) or reconstructing 3D kinematics of virtual body segments from biplanar fluoroscopic video recordings (Baier & Gatesy, 2013), and determining forelimb inertial properties using MRI imaging (Brown et al., 2020; Martin et al., 1989), we focused on the sagittal plane in which most of cat body progression occurs as a first step in analysing forelimb sensorimotor functions in locomotion. As a result, we excluded from our analysis six muscles with the primary actions outside the sagittal plane (APL, ECU, EDLAT2, EDLAT3, EDLAT4 and EDLAT5; Fig. 1A) and neglected the smaller contribution of most forelimb flexors and extensors to adduction–abduction and internal–external rotation moments of force. However, we derived potential functional significance of forelimb muscle morphology for muscle actions outside the sagittal plane based on our morphological measurements (see below).

Another limitation of this study is the use of the regression equations for computing proprioceptive activity of cat forelimb muscles using the instantaneous muscle fascicle length, velocity and activation (Prochazka, 1999; Prochazka & Gorassini, 1998). These equations were developed based on *in vivo* recordings of the afferent activity and mechanical variables of cat hindlimb muscles during locomotion. Thus, they might not fully generalize to forelimb muscles and other behaviours, and their predictive power appears lower than in mechanistic biophysical models of muscle proprioceptors (Blum et al., 2020; Housley et al., 2024; Mileusnic & Loeb, 2006; Mileusnic et al., 2006). Besides complex mechanics, innervation and encoding characteristics of the muscle spindles and Golgi tendon organs, additional factors might affect proprioceptive inputs to the spinal cord and modulation of motoneuronal activity. These factors include the distribution of these receptors within and between MTUs, muscle size, fibre-type composition, muscle location in the body, muscle spindle fusimotor activity and presynaptic inhibition (Banks, 2006; Banks et al., 2009; De Luca & Kline, 2012; Manuel & Zytnicki, 2011; Rudomin, 1999). Given the complexity of factors affecting proprioceptive activity during locomotion, the use of the empirical regression equations relating the afferent activity of muscles with their instantaneous length, velocity, activation and force appears to be a reasonable compromise between accuracy and affordability.

Functional significance of cat forelimb morphology

Morphology comparison between cat forelimbs and hindlimbs. Morphological data of the cat forelimb were obtained to better understand the role of forelimb muscles in generating motor output and sensory feedback during locomotion. A comparison of cat forelimb morphological characteristics with corresponding data of the hindlimb (Sacks & Roy, 1982) revealed a number of similar and contrasting features that support the functional specializations of the two limbs. Muscle mass of the cat forelimb (Fig. 3A and Table 5) and hindlimb (Sacks & Roy, 1982) is concentrated proximally, which contributes to reducing the limb moment of inertia with respect to the proximal joints and energy expenditure required to transport the leg during the swing phase (see 'Introduction'). PCSAs also decline in a proximal–distal direction in the forelimb (Fig. 3B and Table 5), but are more equally distributed in the hindlimb (Sacks & Roy, 1982). The total mass and PCSA of the shoulder protractors (anatomically analogous to hip flexors) is 3–4 times greater than mass and PCSA of shoulder retractors (Fig. 3A and B), although this imbalance would probably be lessened by inclusion of extrinsic shoulder muscles like latissimus dorsi and

pectoralis major. The hip flexors in the cat are smaller and weaker than the hip extensors (Sacks & Roy, 1982). The discrepancy in PCSA and muscle mass, which is proportional to muscle volume or the product of mean PCSA and muscle fascicle length, can be explained by the unique role of the shoulder protractors in supporting body weight in stance and absorbing mechanical energy of the body during walking at constant speed. This is reflected in a greater area of the negative force impulse of the horizontal ground reaction force F_x compared to the positive one (Fig. 4F). Note that muscle volume indicates the maximum amount of positive work (or generated energy) or negative work (absorbed energy) the muscle can do because PCSA is proportional to the muscle's maximum isometric force (Powell et al., 1984), and fascicle length is proportional to the length range of active force production. Thus, shoulder protractors are well suited to absorb energy of the body during stance when these muscles produce the resultant protraction moment of force at the shoulder (Fig. 4G; see also Fig. 7A–C) and are increasing in length for the first two-thirds of stance (Fig. 5A and B). Elbow extensors and wrist plantarflexors do not contribute substantially to energy absorption, or body deceleration, during stance because there is a very limited joint angle yield in early stance at these joints (Fig. 4B and C) and corresponding lengthening of these muscles (Fig. 5A and B). The analogous knee and ankle joints of the cat hindlimb have much more profound joint yield and energy absorption in early stance (McFadyen et al., 1999; Prilutsky et al., 2011).

In addition, the total mass of forelimb muscles was substantially smaller than that of the hindlimb, that is, 139.8 g, Table 5 *vs*. 231.7 g, Table 1 in Sacks & Roy (1982), and thus can contribute less to energy generation for propulsion in locomotion and jumping. The shoulder adductor, abductor and protractor muscles have substantial force generating capacities (large PCSA) compared to the retractors (Fig. 3B). Hindlimb adductors, in contrast, have substantially smaller total PCSA than hip extensors. These differences may reflect the requirement for rapid non-sagittal force production and movements of the forelimbs for lateral balance control in locomotion (Park et al., 2019) and landing (McKinley et al., 1983), as well as defensive fighting or prey capture.

We found considerable variability in fascicle length between forelimb functional MTU groups, for example, flexors and extensors *vs*. adductors, supinators and pronators (Fig. 3C), and within groups, for example, brachioradialis (BCD, 89.6 mm) *vs*. brachialis (BR, 32.4 mm) for elbow flexors (Table 5). Similar variability was observed in the cat hindlimb, for example, soleus (41.7 mm) *vs*. plantaris (18.7 mm) for ankle extensors (Sacks & Roy, 1982). The within-group variation of fascicle length can support functional diversity. One special case, BCD, an elbow flexor and forearm supinator with low force producing potential (PCSA = 0.08 cm^2, more than an order of magnitude smaller than in its synergists; Table 5) has substantially longer fascicles than major elbow flexors or supinators. The BCD may bear some similarity to the abductor cruris caudalis or tenuissimus in the hindlimb (Lev-Tov et al., 1988). Both muscles span several joints/DOFs and their small PCSA indicates that they produce little force. The sensory functions of these muscles may be more important, as they could signal whole limb length (note the pattern similarity between the forelimb length (Fig. 4D) and the BCD MTU length (Fig. 5A) and estimated spindle group II activity (Fig. 9B) during the walking cycle).

Role of the forelimb in weight support and postural control. Weight support during quiet standing requires relatively low force production over a long period with little postural change. This may be particularly true for the cat forelimb, which remains rigid and extended during perturbations of quiet standing (Lacquaniti & Maioli, 1994) and may transfer substantial load through bony structures. The forelimb and hindlimb both possess muscles with predominantly slow-twitch fibre types. The ankle extensor soleus is composed of 100% slow fibres (Ariano et al., 1973), and the ANC and TMED contain 100% and 83% slow-twitch fibres, respectively (Collatos et al., 1977). These antigravity muscles are therefore mechanically and metabolically suited for postural tasks. During horizontal perturbations of the support surface, the hindlimbs exhibit anisotropic force responses in which the greatest stiffness lies backward and outward, while the forelimbs exhibit similar magnitudes of force response in all directions (Honeycutt & Nichols, 2010; Macpherson, 1988). The greater isotropy in force production potential among the shoulder protractors, adductors and abductors (Fig. 3B) compared to corresponding muscles at the hip may explain at least in part the more radially symmetric force responses of the forelimb to postural perturbations. This supports the idea that the forelimbs function primarily as struts during postural control (Lacquaniti & Maioli, 1994; Rushmer et al., 1983).

Role of the forelimb in locomotion. The requirements for locomotion include weight-support, propulsion, balance control and mechanisms for rapid change of direction. Previous work contrasted the forelimbs of the hare (Williams et al., 2007) and cheetah (Hudson et al., 2011a), specialized for rapid changes in direction and speed, with the greyhound (Williams et al., 2008), specialized for straight-line sprinting. The forelimb of the cat, like the forelimb of the hare and cheetah, appears especially well suited for weight-support, stability control and turning. Unlike the greyhound, which has nearly equal distribution of muscle mass between the forelimbs and hindlimbs (the

forelimb muscles are only 11% lighter), the mass of the forelimb muscles in the cat is 60% of the hindlimb muscles – our Table 5 and Table 1 in Sacks & Roy (1982). This suggests a much lower total power generating capacity of the forelimbs and a limited contribution to propulsion. The cat, like the hare (Williams et al., 2007) and the cheetah (Hudson et al., 2011a,b), displays substantial isotropy for PCSA among the protractors, adductors and abductors at the shoulder (Fig. 3B and Table 5). This lack of specialization for protraction–retraction suggests that forelimb adductors and abductors, which are co-active during stance (English, 1978a, b), can produce relatively greater mediolateral forces, providing stability and control of direction during stance. The relatively large PCSA of shoulder adductors and abductors also contributes to the larger moment arms of these muscles with respect to the corresponding axis of rotation at the shoulder, given that the centroid path of the muscle passes further away from this axis. This in turn leads to greater opposing adduction and abduction moments of force at the shoulder, contributing to lateral stabilization of the forelimb during the stance phase of locomotion. The relative similarity in average fascicle length between protractors–retractors and extensors–flexors at the shoulder and elbow in the cat (Fig. 3C and Table 5) also suggests a lesser requirement for acceleration and propulsion in the forelimb than in the hindlimb, where the powerful quadriceps and triceps surae have fascicles half the length of their antagonists (Sacks & Roy, 1982). Therefore, the above characteristics of the cat forelimb musculature appears to be better suited for lateral stability control and for changing the direction of locomotion than for producing acceleration and power for locomotion.

Role of the forelimb in manipulation. Reaching tasks follow a consistent sequence of elbow flexion and wrist dorsiflexion with shoulder protraction as the cat lifts the limb, followed by elbow extension, as the cat thrusts the limb forward, and supination of the antebrachium and wrist plantarflexion prior to target contact; in the retrieval stage, the wrist dorsiflexes and the elbow flexes, while the limb pronates (Illert, 1996; Yakovenko & Drew, 2015). Of special note is the presence of powerful supination and pronation of the forearm about its long axis, the function that is essentially lacking in the homologous hindlimb segment, the shank. In the distal forelimb, the supinator (SUP) and PT are highly specialized, low-mass muscles with short, highly pennated fascicles (Table 5) that provide high forces needed for prey retrieval and suppression, respectively. In the hindlimb, antigravity muscles have much shorter fascicles than their antagonists, often described as specialization for force production (Lieber & Ward, 2011). This specialization is muted in the forelimb, possibly reflecting the benefit of powerful flexors for prey capture as a counter to the benefit of powerful extensors during pursuit. Non-sagittal movements are also frequently involved in foraging and exploratory movements and prey capture. The relatively larger masses of shoulder abductors and adductors are well suited to these out-of-sagittal-plane movements and provide a general-purpose design for strut-like weight support, controlling balance and direction during locomotion and reaching in many directions.

Contribution of cat forelimb morphology to somatosensory control of locomotion. Motion-dependent proprioceptive input to spinal locomotor networks depends on muscle fascicle length, velocity of stretch and force produced by the MTU (Prochazka, 1999). Several morphological and geometric characteristics of MTUs affect the above mechanical variables. A short muscle fascicle length with respect to tendon length can substantially reduce both the range of length change and stretch velocity of the fascicles during locomotion. This is because the relatively long and elastic tendon takes up a substantial amount of stretch in an active MTU, as observed in the cat's medial gastrocnemius, with short fascicles, but not in its close synergist, the soleus, with much longer fascicles, during the stance phase of level walking (Maas et al., 2009). In the cat hindlimb, proximal MTUs (two-joint hamstrings, sartorius) have much longer muscle fascicles/belly than distal MTUs (triceps surae) (Sacks & Roy, 1982; Scott et al., 1992). These morphological differences support distinct roles of length-dependent sensory input from proximal hip muscles in regulating phase transitions during cat locomotion (Gregor et al., 2006; Kriellaars et al., 1994; Lam & Pearson, 2002; McVea et al., 2005). In the cat forelimb, although on average fascicle length of proximal MTUs is not markedly different from that of more distal MTUs (Fig. 3C), one-joint shoulder retractors (SD, TN) and the two-joint shoulder protractor–elbow flexor BB have relatively long fascicle lengths and low tendon–fascicle length ratios (25.1–46.1 mm and 1.1–2.2, respectively, Table 5). The MTU length (Fig. 5A) and estimated activity of muscle spindle group II afferents (Fig. 9B) of these shoulder retractors and shoulder protractor–elbow flexor reach peak values at the end of swing and stance, respectively. Thus, the length-dependent sensory feedback from these MTUs is a strong candidate for communicating to rhythm-generating spinal networks that the forelimb is approaching phase transitions. Properties of spindle group II afferents are well suited to sense limb position (Banks et al., 2021). The BB's patterns of MTU length (Fig. 5A) and spindle group II activity (Fig. 9B) closely match the pattern of forelimb orientation (Fig. 4E) during the walking cycle. Additionally, lengthening patterns of muscle fascicles and spindles in shoulder retractors

during swing and in BB during stance are not likely to be distorted by their active shortening as these MTUs are not active during the corresponding phases of the walking cycle (English, 1978a, b; Krouchev et al., 2006) (see also Fig. 8A). Two slightly more distant MTUs, the elbow flexor–forearm supinator BCD and the elbow flexor–wrist dorsiflexor ECR, have very long fascicle lengths (89.6 and 47.3 mm; Table 5). Their MTU length patterns (Fig. 5A) and estimated spindle group II activity (Fig. 9B) closely match forelimb length changes during the walking cycle (Fig. 4D). Thus, length-dependent inputs from these two MTUs could provide the nervous system with information about overall limb length.

The forelimb moment arms are greater for shoulder protractors and retractors than for more distal muscles as evident from the muscle path locations with respect to the joint centres (Figs 1A and 5C). This increases MTU length changes for a given change in joint angle, making the muscle spindles in the proximal muscles more sensitive to joint position and motion (Hall & McCloskey, 1983). Thus, the relatively long moment arms and fascicle lengths are morphological characteristics of proximal forelimb muscles that make them well suited for providing limb orientation and angular motion information to the spinal cord.

The limb posture also influences the precision of limb position sense and endpoint position control. The limb posture constrains, to a large extent, the limb endpoint precision and stiffness ellipses, which are perpendicular to each other (Bunderson et al., 2010; Burkholder, 2016; Oh & Prilutsky, 2022).

Group Ib Golgi tendon afferents from ankle extensors transmit load-dependent information to locomotor networks (Duysens & Pearson, 1980; Guertin et al., 1995; Hiebert & Pearson, 1999; Ross & Nichols, 2009). This information affects the timing of the stance–swing transition and regulates the activity of hindlimb extensors. It is currently unknown whether group Ib afferents of forelimb distal extensors produce similar functional effects, although they are likely discharging during stance (Fig. 9C) as these antigravity muscles are active and produce moments of force (Figs 4I and 7A–C).

Future directions

The results of this study are essential for understanding the role of cat forelimb morphology for locomotor sensorimotor functions and in providing important information about the potential role of somatosensory feedback in the neural control of quadrupedal locomotion. Although previous studies established strong effects of forelimb movements and forelimb sensory stimulation on hindlimb movements and reflex responses (Akay et al., 2006; Frigon, 2017; Harnie et al., 2024; Hurteau et al., 2018; Mari et al., 2024; Merlet et al., 2022; Miller et al., 1973; Schomburg et al., 1998), this information has not been incorporated into anatomically and neurophysiologically accurate models of mammalian quadrupedal locomotion. These types of models should be capable of providing mechanistic interpretations and explanations of a wide range of experimental data on mechanics and muscle activity patterns during quadrupedal locomotion, including those resulting from various lesions in the spinal cord (Audet et al., 2023; Danner et al., 2023; Doperalski et al., 2011; Mari et al., 2024; Shepard et al., 2023). Spinal cord injury in people, especially complete injury, remains a major healthcare problem. Translational studies on relatively large animal models, like cats (Frigon, 2020; Gerasimenko et al., 2009), and their detailed neuromechanical models (Markin et al., 2016; Nichols et al., 2016) are indispensable for understanding spinal and somatosensory control of locomotion and for developing new rehabilitation approaches. One new promising rehabilitation method is spinal cord stimulation through implanted epidural or non-invasive transcutaneous dorsal stimulating electrodes that appears to increase excitability of spinal locomotor networks transynaptically by activating somatosensory afferents entering the dorsal horns under the electrodes (Harkema et al., 2011; Lorach et al., 2023; Minassian et al., 2016). The spatiotemporal maps of sensory inputs to cervical spinal segments obtained in this study (Fig. 10B–D) could guide the development of targeted epidural/transcutaneous stimulation to improve locomotor function after injury because cervical stimulation has a strong impact on locomotor activity of leg muscles in humans (Gerasimenko et al., 2015). We plan to incorporate the forelimb musculoskeletal model with that of the hindlimbs (Markin et al., 2016) to develop a neuromechanical model of quadrupedal locomotor control to address the above goals.

Conclusion

In this study we measured morphological characteristics of cat forelimb muscles, including 3D coordinates of MTU origin and attachment points, mass, PCSA, fascicle length and moment arms, recorded forelimb walking mechanics, and computed the activation, force and proprioceptive feedback signals of forelimb muscles during walking. Based on the analysis of the obtained information we suggested the important role of morphological characteristics of proximal forelimb muscles in locomotion. These muscles contribute substantially to dissipating mechanical energy of the body in the sagittal plane, controlling lateral stability, providing sensory information about the overall forelimb length and orientation, and regulating the swing–stance and

stance–swing phase transitions. We will use these findings for the development of biologically accurate neuromechanical models of quadrupedal locomotion to explore the mechanisms of interlimb coordination.

References

Akay, T., McVea, D. A., Tachibana, A., & Pearson, K. G. (2006). Coordination of fore and hind leg stepping in cats on a transversely-split treadmill. *Experimental Brain Research*, **175**(2), 211–222.

An, K. N., Ueba, Y., Chao, E. Y., Cooney, W. P., & Linscheid, R. L. (1983). Tendon excursion and moment arm of index finger muscles. *Journal of Biomechanics*, **16**(6), 419–425.

Anderson, F. C., & Pandy, M. G. (2001). Static and dynamic optimization solutions for gait are practically equivalent. *Journal of Biomechanics*, **34**(2), 153–161.

Andrada, E., Reinhardt, L., Lucas, K., & Fischer, M. S. (2017). Three-dimensional inverse dynamics of the forelimb of Beagles at a walk and trot. *American Journal of Veterinary Research*, **78**(7), 804–817.

Arber, S., & Costa, R. M. (2022). Networking brainstem and basal ganglia circuits for movement. *Nature Reviews Neuroscience*, **23**(6), 342–360.

Ariano, M. A., Edgerton, V. R., & Armstrong, R. B. (1973). Hindlimb muscle fiber populations of five mammals. *Journal of Histochemistry and Cytochemistry*, **21**(1), 51–55.

Audet, J., Yassine, S., Lecomte, C. G., Mari, S., Soucy, F., Morency, C., Merlet, A. N., Harnie, J., Beaulieu, C., Gendron, L., Rybak, I. A., Prilutsky, B. I., & Frigon, A. (2023). Spinal sensorimotor circuits play a prominent role in hindlimb locomotor recovery after staggered thoracic lateral hemisections but cannot restore posture and interlimb coordination during quadrupedal locomotion in adult cats. *eNeuro*, **10**(6), 0191-23.

Baier, D. B., & Gatesy, S. M. (2013). Three-dimensional skeletal kinematics of the shoulder girdle and forelimb in walking Alligator. *Journal of Anatomy*, **223**(5), 462–473.

Banks, R. W. (2006). An allometric analysis of the number of muscle spindles in mammalian skeletal muscles. *Journal of Anatomy*, **208**(6), 753–768.

Banks, R. W., Ellaway, P. H., Prochazka, A., & Proske, U. (2021). Secondary endings of muscle spindles: Structure, reflex action, role in motor control and proprioception. *Experimental Physiology*, **106**(12), 2339–2366.

Banks, R. W., Hulliger, M., Saed, H. H., & Stacey, M. J. (2009). A comparative analysis of the encapsulated end-organs of mammalian skeletal muscles and of their sensory nerve endings. *Journal of Anatomy*, **214**(6), 859–887.

Blum, K. P., Campbell, K. S., Horslen, B. C., Nardelli, P., Housley, S. N., Cope, T. C., & Ting, L. H. (2020). Diverse and complex muscle spindle afferent firing properties emerge from multiscale muscle mechanics. *eLife*, **9**, e5517.

Brown, J. M., Wickham, J. B., McAndrew, D. J., & Huang, X. F. (2007). Muscles within muscles: Coordination of 19 muscle segments within three shoulder muscles during isometric motor tasks. *Journal of Electromyography and Kinesiology*, **17**(1), 57–73.

Brown, N. P., Bertocci, G. E., Cheffer, K. A., & Howland, D. R. (2018). A three dimensional multiplane kinematic model for bilateral hind limb gait analysis in cats. *PLoS ONE*, **13**(8), e0197837.

Brown, N. P., Bertocci, G. E., States, G. J. R., Levine, G. J., Levine, J. M., & Howland, D. R. (2020). Development of a canine rigid body musculoskeletal computer model to evaluate gait. *Frontiers in Bioengineering and Biotechnology*, **8**, 150.

Buchanan, T. S., Almdale, D. P., Lewis, J. L., & Rymer, W. Z. (1986). Characteristics of synergic relations during isometric contractions of human elbow muscles. *Journal of Neurophysiology*, **56**(5), 1225–1241.

Bunderson, N. E., Bingham, J. T., Hongchul Sohn, M., Ting, L. H., & Burkholder, T. J. (2012). Neuromechanic: A computational platform for simulation and analysis of the neural control of movement. *International Journal for Numerical Methods in Biomedical*, **28**(10), 1015–1027.

Bunderson, N. E., McKay, J. L., Ting, L. H., & Burkholder, T. J. (2010). Directional constraint of endpoint force emerges from hindlimb anatomy. *Journal of Experimental Biology*, **213**(12), 2131–2141.

Burkholder, T. J., & Lieber, R. L. (2001). Sarcomere length operating range of vertebrate muscles during movement. *Journal of Experimental Biology*, **204**(9), 1529–1536.

Burkholder, T. J., & Nichols, T. R. (2000). The mechanical action of proprioceptive length feedback in a model of cat hindlimb. *Motor Control*, **4**(2), 201–220.

Burkholder, T. J., & Nichols, T. R. (2004). Three-dimensional model of the feline hindlimb. *Journal of Morphology*, **261**(1), 118–129.

Burkholder, T. J. (2016). Model-based approaches to understanding musculoskeletal filtering of neural signals. In B. I. Prilutsky & D. H. Edwards (Eds.), *Neuromechanical modeling of posture and locomotion* (pp. 103–120). Springer.

Cabelguen, J. M., Orsal, D., & Perret, C. (1984). Discharges of forelimb spindle primary afferents during locomotor activity in the decorticate cat. *Brain Research*, **306**(1–2), 359–364.

Caicoya, A. G., Illert, M., & Jänike, R. (1999). Monosynaptic Ia pathways at the cat shoulder. *The Journal of Physiology*, **518**(Pt 3), 825–841.

Chang, Y. H., Auyang, A. G., Scholz, J. P., & Nichols, T. R. (2009). Whole limb kinematics are preferentially conserved over individual joint kinematics after peripheral nerve injury. *Journal of Experimental Biology*, **212**(21), 3511–3521.

Charles, J. P., Cappellari, O., Spence, A. J., Hutchinson, J. R., & Wells, D. J. (2016). Musculoskeletal geometry, muscle architecture and functional specialisations of the mouse hindlimb. *PLoS ONE*, **11**(4), e0147669.

Charles, J. P., Cappellari, O., Spence, A. J., Wells, D. J., & Hutchinson, J. R. (2016). Muscle moment arms and sensitivity analysis of a mouse hindlimb musculoskeletal model. *Journal of Anatomy*, **229**(4), 514–535.

Collatos, T. C., Edgerton, V. R., Smith, J. L., & Botterman, B. R. (1977). Contractile properties and fiber type compositions of flexors and extensors of elbow joint in cat: Implications for motor control. *Journal of Neurophysiology*, **40**(6), 1292–1300.

Corbee, R. J., Maas, H., Doornenbal, A., & Hazewinkel, H. A. (2014). Forelimb and hindlimb ground reaction forces of walking cats: Assessment and comparison with walking dogs. *Veterinary Journal*, **202**(1), 116–127.

Crowninshield, R. D., & Brand, R. A. (1981). A physiologically based criterion of muscle force prediction in locomotion. *Journal of Biomechanics*, **14**(11), 793–801.

Danner, S. M., Shepard, C. T., Hainline, C., Shevtsova, N. A., Rybak, I. A., & Magnuson, D. S. K. (2023). Spinal control of locomotion before and after spinal cord injury. *Experimental Neurology*, **368**, 114496.

Danner, S. M., Shevtsova, N. A., Frigon, A., & Rybak, I. A. (2017). Computational modeling of spinal circuits controlling limb coordination and gaits in quadrupeds. *eLife*, **6**, e31050.

De Luca, C. J., & Kline, J. C. (2012). Influence of proprioceptive feedback on the firing rate and recruitment of motoneurons. *Journal of Neural Engineering*, **9**(1), 016007.

Diogo, R., & Molnar, J. (2014). Comparative anatomy, evolution, and homologies of tetrapod hindlimb muscles, comparison with forelimb muscles, and deconstruction of the forelimb-hindlimb serial homology hypothesis. *The Anatomical Record*, **297**(6), 1047–1075.

Doperalski, A. E., Tester, N. J., Jefferson, S. C., & Howland, D. R. (2011). Altered obstacle negotiation after low thoracic hemisection in the cat. *Journal of Neurotrauma*, **28**(9), 1983–1993.

Dougherty, K. J. (2023). Distinguishing subtypes of spinal locomotor neurons to inform circuit function and dysfunction. *Current Opinion in Neurobiology*, **82**, 102763.

Dutto, D. J., Hoyt, D. F., Clayton, H. M., Cogger, E. A., & Wickler, S. J. (2006). Joint work and power for both the forelimb and hindlimb during trotting in the horse. *Journal of Experimental Biology*, **209**(20), 3990–3999.

Dutto, D. J., Hoyt, D. F., Cogger, E. A., & Wickler, S. J. (2004). Ground reaction forces in horses trotting up an incline and on the level over a range of speeds. *Journal of Experimental Biology*, **207**(20), 3507–3514.

Duysens, J., & Pearson, K. G. (1980). Inhibition of flexor burst generation by loading ankle extensor muscles in walking cats. *Brain Research*, **187**(2), 321–332.

Eccles, J. C., Eccles, R. M., Iggo, A., & Ito, M. (1961). Distribution of recurrent inhibition among motoneurones. *The Journal of physiology*, **159**(3), 479–499.

Eccles, J. C., Eccles, R. M., & Lundberg, A. (1957a). The convergence of monosynaptic excitatory afferents on to many different species of alpha motoneurones. *The Journal of Physiology*, **137**(1), 22–50.

Eccles, J. C., Eccles, R. M., & Lundberg, A. (1957b). Synaptic actions on motoneurones caused by impulses in Golgi tendon organ afferents. *The Journal of Physiology*, **138**(2), 227–252.

Eccles, R. M., & Lundberg, A. (1958). Integrative pattern of Ia synaptic actions on motoneurones of hip and knee muscles. *The Journal of Physiology*, **144**(2), 271–298.

Edgley, S., Jankowska, E., & McCrea, D. (1986). The heteronymous monosynaptic actions of triceps surae group Ia afferents on hip and knee extensor motoneurones in the cat. *Experimental Brain Research*, **61**(2), 443–446.

Ekeberg, O., & Pearson, K. (2005). Computer simulation of stepping in the hind legs of the cat: An examination of mechanisms regulating the stance-to-swing transition. *Journal of Neurophysiology*, **94**(6), 4256–4268.

Elftman, H. (1940). Work done by muscles in running. *American Journal of Physiology*, **129**(3), 672–684.

English, A. W. (1978a). An electromyographic analysis of forelimb muscles during overground stepping in the cat. *Journal of Experimental Biology*, **76**(1), 105–122.

English, A. W. (1978b). Functional analysis of the shoulder girdle of cats during locomotion. *Journal of Morphology*, **156**(2), 279–292.

English, A. W., & Weeks, O. I. (1987). An anatomical and functional analysis of cat biceps femoris and semitendinosus muscles. *Journal of Morphology*, **191**(2), 161–175.

Farrell, B. J., Bulgakova, M. A., Beloozerova, I. N., Sirota, M. G., & Prilutsky, B. I. (2014). Body stability and muscle and motor cortex activity during walking with wide stance. *Journal of Neurophysiology*, **112**(3), 504–524.

Farrell, B. J., Bulgakova, M. A., Sirota, M. G., Prilutsky, B. I., & Beloozerova, I. N. (2015). Accurate stepping on a narrow path: Mechanics, EMG, and motor cortex activity in the cat. *Journal of Neurophysiology*, **114**(5), 2682–2702.

Fischer, M. S., & Blickhan, R. (2006). The tri-segmented limbs of therian mammals: Kinematics, dynamics, and self-stabilization–a review. *Journal of Experimental Zoology Part A, Comparative Experimental Biology*, **305A**(11), 935–952.

flax. (2022). Global Sensitivity Analysis Toolbox, pp. https://www.mathworks.com/matlabcentral/fileexchange/40759-global-sensitivity-analysis-toolbox. MATLAB Central File Exchange.

Frigon, A. (2017). The neural control of interlimb coordination during mammalian locomotion. *Journal of Neurophysiology*, **117**(6), 2224–2241.

Frigon, A., Akay, T., & Prilutsky, B. I. (2022). Control of mammalian locomotion by somatosensory feedback. *Comparative Physiology*, **12**, 2877–2947.

Frigon, A. (2020). Fundamental contributions of the cat model to the neural control of locomotion. In: P. J. Whelan & S. A. Sharples (Eds.), *The neural control of movement* (pp. 315–348). Academic Press.

Fritz, N., Illert, M., de la Motte, S., Reeh, P., & Saggau, P. (1989). Pattern of monosynaptic Ia connections in the cat forelimb. *The Journal of Physiology*, **419**(1), 321–351.

Fritz, N., Illert, M., & Reeh, P. (1986). Location of motoneurones projecting to the cat distal forelimb. II. Median and ulnar motornuclei. *The Journal of Comparative Neurology*, **244**(3), 302–312.

Fritz, N., Illert, M., & Saggau, P. (1986). Location of motoneurones projecting to the cat distal forelimb. I. Deep radial motornuclei. *The Journal of Comparative Neurology*, **244**(3), 286–301.

Gambaryan, P. P. (1974). *How animals run: Anatomical adaptations*. John Wiley and Sons.

Gerasimenko, Y., Gorodnichev, R., Puhov, A., Moshonkina, T., Savochin, A., Selionov, V., Roy, R. R., Lu, D. C., & Edgerton, V. R. (2015). Initiation and modulation of locomotor circuitry output with multisite transcutaneous electrical stimulation of the spinal cord in noninjured humans. *Journal of Neurophysiology*, **113**(3), 834–842.

Gerasimenko, Y., Musienko, P., Bogacheva, I., Moshonkina, T., Savochin, A., Lavrov, I., Roy, R. R., & Edgerton, V. R. (2009). Propriospinal bypass of the serotonergic system that can facilitate stepping. *The Journal of Neuroscience*, **29**(17), 5681–5689.

Gonyea, W. J., Marushia, S. A., & Dixon, J. A. (1981). Morphological organization and contractile properties of the wrist flexor muscles in the cat. *The Anatomical Record*, **199**(3), 321–339.

Goslow, G. E., Jr., Reinking, R. M., & Stuart, D. G. (1973). The cat step cycle: Hind limb joint angles and muscle lengths during unrestrained locomotion. *Journal of Morphology*, **141**(1), 1–41.

Graham, K. M., & Scott, S. H. (2003). Morphometry of Macaca mulatta forelimb. III. Moment arm of shoulder and elbow muscles. *Journal of Morphology*, **255**(3), 301–314.

Gray, J. (1944). Studies in the mechanics of the tetrapod skeleton. *Journal of Experimental Biology*, **20**(2), 88–116.

Gregersen, C. S., Silverton, N. A., & Carrier, D. R. (1998). External work and potential for elastic storage at the limb joints of running dogs. *Journal of Experimental Biology*, **201**(23), 3197–3210.

Gregor, R. J., Maas, H., Bulgakova, M. A., Oliver, A., English, A. W., & Prilutsky, B. I. (2018). Time course of functional recovery during the first 3 mo after surgical transection and repair of nerves to the feline soleus and lateral gastrocnemius muscles. *Journal of Neurophysiology*, **119**(3), 1166–1185.

Gregor, R. J., Smith, D. W., & Prilutsky, B. I. (2006). Mechanics of slope walking in the cat: Quantification of muscle load, length change, and ankle extensor EMG patterns. *Journal of Neurophysiology*, **95**(3), 1397–1409.

Grillner, S., & El Manira, A. (2020). Current principles of motor control, with special reference to vertebrate locomotion. *Physiological Reviews*, **100**(1), 271–320.

Guertin, P., Angel, M. J., Perreault, M. C., & McCrea, D. A. (1995). Ankle extensor group I afferents excite extensors throughout the hindlimb during fictive locomotion in the cat. *The Journal of Physiology*, **487**(Pt 1), 197–209.

Hall, L. A., & McCloskey, D. I. (1983). Detections of movements imposed on finger, elbow and shoulder joints. *The Journal of Physiology*, **335**(1), 519–533.

Harkema, S., Gerasimenko, Y., Hodes, J., Burdick, J., Angeli, C., Chen, Y., Ferreira, C., Willhite, A., Rejc, E., Grossman, R. G., & Edgerton, V. R. (2011). Effect of epidural stimulation of the lumbosacral spinal cord on voluntary movement, standing, and assisted stepping after motor complete paraplegia: A case study. *The Lancet*, **377**(9781), 1938–1947.

Harnie, J., Al Arab, R., Mari, S., Yassine, S., Eddaoui, O., Jéhannin, P., Audet, J., Lecomte, C., Iorio-Morin, C., Prilutsky, B. I., Rybak, I. A., & Frigon, A. (2024). Forelimb movements contribute to hindlimb cutaneous reflexes during locomotion in cats. *Journal of Neurophysiology*, **131**(6), 997–1013.

Haruno, M., & Wolpert, D. M. (2005). Optimal control of redundant muscles in step-tracking wrist movements. *Journal of Neurophysiology*, **94**(6), 4244–4255.

He, J., Levine, W. S., & Loeb, G. E. (1991). Feedback gains for correcting small perturbations to standing posture. *IEEE Transactions on Automative Control*, **36**(3), 322–332.

Hiebert, G. W., & Pearson, K. G. (1999). Contribution of sensory feedback to the generation of extensor activity during walking in the decerebrate cat. *Journal of Neurophysiology*, **81**(2), 758–770.

Honeycutt, C. F., & Nichols, T. R. (2010). The decerebrate cat generates the essential features of the force constraint strategy. *Journal of Neurophysiology*, **103**(6), 3266–3273.

Hörner, M., & Kümmel, H. (1993). Topographical representation of shoulder motor nuclei in the cat spinal cord as revealed by retrograde fluorochrome tracers. *The Journal of Comparative Neurology*, **335**(3), 309–319.

Housley, S. N., Powers, R. K., Nardelli, P., Lee, S., Blum, K., Bewick, G. S., Banks, R. W., & Cope, T. C. (2024). Biophysical model of muscle spindle encoding. *Experimental Physiology*, **109**(1), 55–65.

Hoy, M. G., & Zernicke, R. F. (1985). Modulation of limb dynamics in the swing phase of locomotion. *Journal of Biomechanics*, **18**(1), 49–60.

Hudson, P. E., Corr, S. A., Payne-Davis, R. C., Clancy, S. N., Lane, E., & Wilson, A. M. (2011a). Functional anatomy of the cheetah (Acinonyx jubatus) forelimb. *Journal of Anatomy*, **218**(4), 375–385.

Hudson, P. E., Corr, S. A., Payne-Davis, R. C., Clancy, S. N., Lane, E., & Wilson, A. M. (2011b). Functional anatomy of the cheetah (Acinonyx jubatus) hindlimb. *Journal of Anatomy*, **218**(4), 363–374.

Hug, F., Avrillon, S., Ibanez, J., & Farina, D. (2022). Common synaptic input, synergies and size principle: Control of spinal motor neurons for movement generation. *The Journal of Physiology*, **601**(15), 3201–3219.

Hurteau, M. F., Thibaudier, Y., Dambreville, C., Danner, S. M., Rybak, I. A., & Frigon, A. (2018). Intralimb and Interlimb Cutaneous Reflexes during Locomotion in the Intact Cat. *The Journal of Neuroscience*, **38**(17), 4104–4122.

Illert, M. (1996). Monosynaptic Ia pathways and motor behaviour of the cat distal forelimb. *Acta Neurobiologiae Experimentalis*, **56**(1), 423–434.

Illert, M., & Wietelmann, D. (1989). Distribution of recurrent inhibition in the cat forelimb. *Progress in Brain Research*, **80**, 273–281. discussion 269–271.

Ivanenko, Y. P., Poppele, R. E., & Lacquaniti, F. (2006). Spinal cord maps of spatiotemporal alpha-motoneuron activation in humans walking at different speeds. *Journal of Neurophysiology*, **95**(2), 602–618.

Jarrell, J. R., Farrell, B. J., Kistenberg, R. S., Dalton, J. F., Pitkin, M., & Prilutsky, B. I. (2018). Kinetics of individual limbs during level and slope walking with a unilateral transtibial bone-anchored prosthesis in the cat. *Journal of Biomechanics*, **76**, 74–83.

Jenny, A. B., & Inukai, J. (1983). Principles of motor organization of the monkey cervical spinal cord. *The Journal of Neuroscience*, **3**(3), 567–575.

Kibleur, P., Tata, S. R., Greiner, N., Conti, S., Barra, B., Zhuang, K., Kaeser, M., Ijspeert, A., & Capogrosso, M. (2020). Spatiotemporal maps of proprioceptive inputs to the cervical spinal cord during three-dimensional reaching and grasping. *IEEE Transactions on Neural Systems and Rehabilitation Engineering*, **28**(7), 1668–1677.

Kilbourne, B. M., & Carrier, D. R. (2016). Manipulated changes in limb mass and rotational inertia in trotting dogs (Canis lupus familiaris) and their effect on limb kinematics. *Journal of Experimental Zoology Part A: Ecological and Integrative Physiology*, **325**(10), 665–674.

Klishko, A. N., Akyildiz, A., Mehta-Desai, R., & Prilutsky, B. I. (2021). Common and distinct muscle synergies during level and slope locomotion in the cat. *Journal of Neurophysiology*, **126**(2), 493–515.

Klishko, A. N., Farrell, B. J., Beloozerova, I. N., Latash, M. L., & Prilutsky, B. I. (2014). Stabilization of cat paw trajectory during locomotion. *Journal of Neurophysiology*, **112**(6), 1376–1391.

Komi, P. V. (2003). Stretch-shortening cycle. In: P. V. Komi (Ed.), *Strength and power in sport the encyclopaedia of sports medicine volume III* (pp. 184–202). Blackwell Science.

Kriellaars, D. J., Brownstone, R. M., Noga, B. R., & Jordan, L. M. (1994). Mechanical entrainment of fictive locomotion in the decerebrate cat. *Journal of Neurophysiology*, **71**(6), 2074–2086.

Krouchev, N., Kalaska, J. F., & Drew, T. (2006). Sequential activation of muscle synergies during locomotion in the intact cat as revealed by cluster analysis and direct decomposition. *Journal of Neurophysiology*, **96**(4), 1991–2010.

Kuznetsov, A. N. (1995). Energetical profit of the third segment in parasagittal legs. *Journal of Theoretical Biology*, **172**(1), 95–105.

Lacquaniti, F., & Maioli, C. (1994). Independent control of limb position and contact forces in cat posture. *Journal of Neurophysiology*, **72**(4), 1476–1495.

Lam, T., & Pearson, K. G. (2001). Proprioceptive modulation of hip flexor activity during the swing phase of locomotion in decerebrate cats. *Journal of Neurophysiology*, **86**(3), 1321–1332.

Lam, T., & Pearson, K. G. (2002). Sartorius muscle afferents influence the amplitude and timing of flexor activity in walking decerebrate cats. *Experimental Brain Research*, **147**(2), 175–185.

Lavoie, S., McFadyen, B., & Drew, T. (1995). A kinematic and kinetic analysis of locomotion during voluntary gait modification in the cat. *Experimental Brain Research*, **106**(1), 39–56.

Lecomte, C. G., Mari, S., Audet, J., Merlet, A. N., Harnie, J., Beaulieu, C., Abdallah, K., Gendron, L., Rybak, I. A., Prilutsky, B. I., & Frigon, A. (2022). Modulation of the gait pattern during split-belt locomotion after lateral spinal cord hemisection in adult cats. *Journal of Neurophysiology*, **128**(6), 1593–1616.

Lecomte, C. G., Mari, S., Audet, J., Yassine, S., Merlet, A. N., Morency, C., Harnie, J., Beaulieu, C., Gendron, L., & Frigon, A. (2023). Neuromechanical strategies for obstacle negotiation during overground locomotion following incomplete spinal cord injury in adult cats. *The Journal of Neuroscience*, **43**(31), 5623–5641.

Leiras, R., Cregg, J. M., & Kiehn, O. (2022). Brainstem circuits for locomotion. *Annual Review of Neuroscience*, **45**(1), 63–85.

Levine, A. J., Lewallen, K. A., & Pfaff, S. L. (2012). Spatial organization of cortical and spinal neurons controlling motor behavior. *Current Opinion in Neurobiology*, **22**(5), 812–821.

Lev-Tov, A., Pratt, C. A., & Burke, R. E. (1988). The motor-unit population of the cat tenuissimus muscle. *Journal of Neurophysiology*, **59**(4), 1128–1142.

Lieber, R. L., & Ward, S. R. (2011). Skeletal muscle design to meet functional demands. *Philosophical Transactions of the Royal Society of London. Series B: Biological Sciences*, **366**(1570), 1466–1476.

Loeb, G. E., & Duysens, J. (1979). Activity patterns in individual hindlimb primary and secondary muscle spindle afferents during normal movements in unrestrained cats. *Journal of Neurophysiology*, **42**(2), 420–440.

Lorach, H., Galvez, A., Spagnolo, V., Martel, F., Karakas, S., Intering, N., Vat, M., Faivre, O., Harte, C., Komi, S., Ravier, J., Collin, T., Coquoz, L., Sakr, I., Baaklini, E., Hernandez-Charpak, S. D., Dumont, G., Buschman, R., Buse, N., … Courtine G. (2023). Walking naturally after spinal cord injury using a brain-spine interface. *Nature*, **618**(7963), 126–133.

Maas, H., Gregor, R. J., Hodson-Tole, E. F., Farrell, B. J., English, A. W., & Prilutsky, B. I. (2010). Locomotor changes in length and EMG activity of feline medial gastrocnemius muscle following paralysis of two synergists. *Experimental Brain Research*, **203**(4), 681–692.

Maas, H., Gregor, R. J., Hodson-Tole, E. F., Farrell, B. J., & Prilutsky, B. I. (2009). Distinct muscle fascicle length changes in feline medial gastrocnemius and soleus muscles during slope walking. *Journal of Applied Physiology*, **106**(4), 1169–1180.

Macpherson, J. M. (1988). Strategies that simplify the control of quadrupedal stance. I. Forces at the ground. *Journal of Neurophysiology*, **60**(1), 204–217.

Manuel, M., & Zytnicki, D. (2011). Alpha, beta and gamma motoneurons: Functional diversity in the motor system's final pathway. *Journal of Integrative Neuroscience*, **10**(03), 243–276.

Mari, S., Lecomte, C. G., Merlet, A. N., Audet, J., Harnie, J., Rybak, I. A., Prilutsky, B. I., & Frigon, A. (2023). A sensory signal related to left-right symmetry modulates intra- and interlimb cutaneous reflexes during locomotion in intact cats. *Frontiers in Systems Neuroscience*, **17**, 1199079.

Mari, S., Lecomte, C. G., Merlet, A. N., Audet, J., Yassine, S., Eddaoui, O., Genois, G., Nadeau, C., Harnie, J., Rybak, I. A., Prilutsky, B. I., & Frigon, A. (2024). Changes in intra- and interlimb reflexes from hindlimb cutaneous afferents after staggered thoracic lateral hemisections during locomotion in cats. *The Journal of Physiology*, **602**(9), 1987–2017.

Markin, S. N., Klishko, A. N., Shevtsova, N. A., Lemay, M. A., Prilutsky, B. I., & Rybak, I. A. (2016). A neuromechanical model of spinal control of locomotion. In B. I. Prilutsky & D. H. Edwards, Jr (Eds.), *Neuromechanical modeling of posture and locomotion* (pp. 21–65). Springer.

Martin, P. E., Mungiole, M., Marzke, M. W., & Longhill, J. M. (1989). The use of magnetic resonance imaging for measuring segment inertial properties. *Journal of Biomechanics*, **22**(4), 367–376.

Martin, R., Tan, C., Burkholder, T. J., & Nichols, T. R. (2010). Construction of a musculoskeletal model of the cat forelimb. In *Society for Neuroscience Annual Meeting Program number 38119*. San Diego, CA.

Mathewson, M. A., Chapman, M. A., Hentzen, E. R., Fridén, J., & Lieber, R. L. (2012). Anatomical, architectural, and biochemical diversity of the murine forelimb muscles. *Journal of Anatomy*, **221**(5), 443–451.

McFadyen, B. J., Lavoie, S., & Drew, T. (1999). Kinetic and energetic patterns for hindlimb obstacle avoidance during cat locomotion. *Experimental Brain Research*, **125**(4), 502–510.

McKinley, P. A., Smith, J. L., & Gregor, R. J. (1983). Responses of elbow extensors to landing forces during jump downs in cats. *Experimental Brain Research*, **49**(2), 218–228.

McVea, D. A., Donelan, J. M., Tachibana, A., & Pearson, K. G. (2005). A role for hip position in initiating the swing-to-stance transition in walking cats. *Journal of Neurophysiology*, **94**(5), 3497–3508.

Merlet, A. N., Jéhannin, P., Mari, S., Lecomte, C. G., Audet, J., Harnie, J., Rybak, I. A., Prilutsky, B. I., & Frigon, A. (2022). Sensory perturbations from hindlimb cutaneous afferents generate coordinated functional responses in all four limbs during locomotion in intact cats. *eNeuro*, **9**(6), ENEURO.0178-22.2022.

Mileusnic, M. P., Brown, I. E., Lan, N., & Loeb, G. E. (2006). Mathematical models of proprioceptors. I. Control and transduction in the muscle spindle. *Journal of Neurophysiology*, **96**(4), 1772–1788.

Mileusnic, M. P., & Loeb, G. E. (2006). Mathematical models of proprioceptors. II. Structure and function of the Golgi tendon organ. *Journal of Neurophysiology*, **96**(4), 1789–1802.

Miller, S., Reitsma, D. J., & van der Meché, F. G. (1973). Functional organization of long ascending propriospinal pathways linking lumbo-sacral and cervical segments in the cat. *Brain Research*, **62**(1), 169–188.

Miller, S., & Van Der Meché, F. G. A. (1975). Movements of the forelimbs of the cat during stepping on a treadmill. *Brain Research*, **91**(2), 255–269.

Minassian, K., Hofstoetter, U. S., Danner, S. M., Mayr, W., Bruce, J. A., McKay, W. B., & Tansey, K. E. (2016). Spinal rhythm generation by step-induced feedback and transcutaneous posterior root stimulation in complete spinal cord-injured individuals. *Neurorehabilitation and Neural Repair*, **30**(3), 233–243.

Neptune, R. R., Sasaki, K., & Kautz, S. A. (2008). The effect of walking speed on muscle function and mechanical energetics. *Gait & Posture*, **28**(1), 135–143.

Nichols, T. R. (1994). A biomechanical perspective on spinal mechanisms of coordinated muscular action: An architecture principle. *Acta Anatomica*, **151**(1), 1–13.

Nichols, T. R. (1999). Receptor mechanisms underlying heterogenic reflexes among the triceps surae muscles of the cat. *Journal of Neurophysiology*, **81**(2), 467–478.

Nichols, T. R. (2018). Distributed force feedback in the spinal cord and the regulation of limb mechanics. *Journal of Neurophysiology*, **119**(3), 1186–1200.

Nichols, T. R., Bunderson, N., & Lyle, M. (2016). Neural regulation of limb mechanics: Insights from the organization of proprioceptive circuits. In B. I. Prilutsky & D.H. Edwards, Jr (Eds.), *Neuromechanical Modeling of Posture and Locomotion* (pp. 69–102). Springer.

Oh, K., & Prilutsky, B. I. (2022). Transformation from arm joint coordinates to hand external coordinates explains non-uniform precision of hand position sense in horizontal workspace. *Human Movement Science*, **86**, 103020.

Pandy, M. G., Kumar, V., Berme, N., & Waldron, K. J. (1988). The dynamics of quadrupedal locomotion. *Journal of Biomechanical Engineering*, **110**(3), 230–237.

Pantall, A., Gregor, R. J., & Prilutsky, B. I. (2012). Stance and swing phase detection during level and slope walking in the cat: Effects of slope, injury, subject and kinematic detection method. *Journal of Biomechanics*, **45**(8), 1529–1533.

Park, H., Klishko, A. N., Oh, K., Zhang, C., Grenga, G., Herrin, K. R., Dalton, J. F., Kistenberg, R. S., Lemay, M. A., Pitkin, M., DeWeerth, S. P., & Prilutsky, B. I. (2023). Electrical stimulation of distal tibial nerve during stance phase of walking may reverse effects of unilateral paw pad anesthesia in the cat. *Motor Control*, **27**(1), 71–95.

Park, H., Latash, E. M., Molkov, Y. I., Klishko, A. N., Frigon, A., DeWeerth, S. P., & Prilutsky, B. I. (2019). Cutaneous sensory feedback from paw pads affects lateral balance control during split-belt locomotion in the cat. *Journal of Experimental Biology*, **222**(14), jeb198648.

Percie Du Sert, N., Hurst, V., Ahluwalia, A., Alam, S., Avey, M. T., Baker, M., Browne, W. J., Clark, A., Cuthill, I. C., Dirnagl, U., Emerson, M., Garner, P., Holgate, S. T., Howells, D. W., Karp, N. A., Lazic, S. E., Lidster, K., Maccallum, C. J., Macleod, M., … Würbel, H. (2020). The ARRIVE guidelines 2.0: Updated guidelines for reporting animal research. *PLoS Biology*, **18**(7), e3000410.

Powell, P. L., Roy, R. R., Kanim, P., Bello, M. A., & Edgerton, V. R. (1984). Predictability of skeletal muscle tension from architectural determinations in guinea pig hindlimbs. *Journal of Applied Physiology: Respiratory, Environmental and Exercise Physiology*, **57**(6), 1715–1721.

Prado, L. G., Makarenko, I., Andresen, C., Kruger, M., Opitz, C. A., & Linke, W. A. (2005). Isoform diversity of giant proteins in relation to passive and active contractile properties of rabbit skeletal muscles. *Journal of General Physiology*, **126**(5), 461–480.

Prilutsky, B. I. (2000a). Coordination of two- and one-joint muscles: Functional consequences and implications for motor control. *Motor Control*, **4**(1), 1–44.

Prilutsky, B. I. (2000b). Muscle coordination: The discussion continues. *Motor Control*, **4**(1), 97–116.

Prilutsky, B. I., Herzog, W., & Allinger, T. L. (1997). Forces of individual cat ankle extensor muscles during locomotion predicted using static optimization. *Journal of Biomechanics*, **30**(10), 1025–1033.

Prilutsky, B. I., Klishko, A. N., Weber, D. J., & Lemay, M. A. (2016). Computing motion dependent afferent activity during cat locomotion using a forward dynamics musculoskeletal model. In B. I. Prilutsky & D. H. Edwards, Jr (Eds.), *Neuromechanical modeling of posture and locomotion* (pp. 273–307). Springer.

Prilutsky, B. I., Maas, H., Bulgakova, M., Hodson-Tole, E. F., & Gregor, R. J. (2011). Short-term motor compensations to denervation of feline soleus and lateral gastrocnemius result in preservation of ankle mechanical output during locomotion. *Cells Tissues Organs*, **193**(5), 310–324.

Prilutsky, B. I., Parker, J., Cymbalyuk, G. S., & Klishko, A. N. (2022). Emergence of extreme paw accelerations during cat paw shaking: Interactions of spinal central pattern generator, hindlimb mechanics and muscle length-depended feedback. *Frontiers in Integrative Neuroscience*, **16**, 810139.

Prilutsky, B. I., Sirota, M. G., Gregor, R. J., & Beloozerova, I. N. (2005). Quantification of motor cortex activity and full-body biomechanics during unconstrained locomotion. *Journal of Neurophysiology*, **94**(4), 2959–2969.

Prilutsky, B. I., & Zatsiorsky, V. M. (2002). Optimization-based models of muscle coordination. *Exercise and Sport Sciences Reviews*, **30**(1), 32–38.

Prochazka, A. (1999). Quantifying proprioception. *Progress in Brain Research*, **123**, 133–142.

Prochazka, A., & Gorassini, M. (1998). Ensemble firing of muscle afferents recorded during normal locomotion in cats. *The Journal of Physiology*, **507**(Pt 1), 293–304.

Qian, G., & Mahdi, A. (2020). Sensitivity analysis methods in the biomedical sciences. *Mathematical Biosciences*, **323**, 108306.

Raikova, R. T., & Prilutsky, B. I. (2001). Sensitivity of predicted muscle forces to parameters of the optimization-based human leg model revealed by analytical and numerical analyses. *Journal of Biomechanics*, **34**(10), 1243–1255.

Ross, K. T., & Nichols, T. R. (2009). Heterogenic feedback between hindlimb extensors in the spontaneously locomoting premammillary cat. *Journal of Neurophysiology*, **101**(1), 184–197.

Rothier, P. S., Fabre, A. C., Clavel, J., Benson, R. B. J., & Herrel, A. (2023). Mammalian forelimb evolution is driven by uneven proximal-to-distal morphological diversity. *eLife*, **12**, e81492.

Rudomin, P. (1999). Presynaptic selection of afferent inflow in the spinal cord. *Journal of Physiology, Paris*, **93**(4), 329–347.

Rushmer, D. S., Russell, C. J., Macpherson, J., Phillips, J. O., & Dunbar, D. C. (1983). Automatic postural responses in the cat: Responses to headward and tailward translation. *Experimental Brain Research*, **50**(1), 45–61.

Sacks, R. D., & Roy, R. R. (1982). Architecture of the hind limb muscles of cats: Functional significance. *Journal of Morphology*, **173**(2), 185–195.

Schomburg, E. D., Petersen, N., Barajon, I., & Hultborn, H. (1998). Flexor reflex afferents reset the step cycle during fictive locomotion in the cat. *Experimental Brain Research*, **122**(3), 339–350.

Scott, S. H., Thomson, D. B., Richmond, F. J., & Loeb, G. E. (1992). Neuromuscular organization of feline anterior sartorius: II. Intramuscular length changes and complex length-tension relationships during stimulation of individual nerve branches. *Journal of Morphology*, **213**(2), 171–183.

Scott, S. H., Brown, I. E., & Loeb, G. E. (1996). Mechanics of feline soleus: I. Effect of fascicle length and velocity on force output. *Journal of Muscle Research and Cell Motility*, **17**(2), 207–219.

Shepard, C. T., Brown, B. L., Van Rijswijck, M. A., Zalla, R. M., Burke, D. A., Morehouse, J. R., Riegler, A. S., Whittemore, S. R., & Magnuson, D. S. K. (2023). Silencing long-descending inter-enlargement propriospinal neurons improves hindlimb stepping after contusive spinal cord injuries. *eLife*, **12**, e82944.

Shubin, N., Tabin, C., & Carroll, S. (1997). Fossils, genes and the evolution of animal limbs. *Nature*, **388**(6643), 639–648.

Singh, K., Melis, E. H., Richmond, F. J., & Scott, S. H. (2002). Morphometry of Macaca mulatta forelimb. II. Fiber-type composition in shoulder and elbow muscles. *Journal of Morphology*, **251**(3), 323–332.

Sobol′, I. M. (2001). Global sensitivity indices for nonlinear mathematical models and their Monte Carlo estimates. *Mathematics and Computers in Simulation*, **55**(1–3), 271–280.

Spector, S. A., Gardiner, P. F., Zernicke, R. F., Roy, R. R., & Edgerton, V. R. (1980). Muscle architecture and force-velocity characteristics of cat soleus and medial gastrocnemius: Implications for motor control. *Journal of Neurophysiology*, **44**(5), 951–960.

Stark, H., Fischer, M. S., Hunt, A., Young, F., Quinn, R., & Andrada, E. (2021). A three-dimensional musculoskeletal model of the dog. *Scientific Reports*, **11**(1), 11335.

Sterling, P., & Kuypers, H. G. (1967a). Anatomical organization of the brachial spinal cord of the cat. I. The distribution of dorsal root fibers. *Brain Research*, **4**(1), 1–15.

Sterling, P., & Kuypers, H. G. (1967b). Anatomical organization of the brachial spinal cord of the cat. II. The motoneuron plexus. *Brain Research*, **4**(1), 16–32.

Tata Ramalingasetty, S., Danner, S. M., Arreguit, J., Markin, S. N., Rodarie, D., Kathe, C., Courtine, G., Rybak, I. A., & Ijspeert, A. J. (2021). A whole-body musculoskeletal model of the mouse. *IEEE Access*, **9**, 163861–163881.

Turkin, V. V., Monroe, K. S., & Hamm, T. M. (1998). Organization of recurrent inhibition and facilitation in motor nuclei innervating ankle muscles of the cat. *Journal of Neurophysiology*, **79**(2), 778–790.

Van Ingen Schenau, G. J., Pratt, C. A., & Macpherson, J. M. (1994). Differential use and control of mono- and biarticular muscles. *Human Movement Science*, **13**(3–4), 495–517.

Veldpaus, F. E., Woltring, H. J., & Dortmans, L. J. (1988). A least-squares algorithm for the equiform transformation from spatial marker co-ordinates. *Journal of Biomechanics*, **21**(1), 45–54.

Watt, P. W., Kelly, F. J., Goldspink, D. F., & Goldspink, G. (1982). Exercise-induced morphological and biochemical changes in skeletal muscles of the rat. *Journal of Applied Physiology-Respiratory, Environmental and Exercise Physiology*, **53**(5), 1144–1151.

Williams, S. B., Wilson, A. M., Daynes, J., Peckham, K., & Payne, R. C. (2008). Functional anatomy and muscle moment arms of the thoracic limb of an elite sprinting athlete: The racing greyhound (Canis familiaris). *Journal of Anatomy*, **213**(4), 373–382.

Williams, S. B., Wilson, A. M., & Payne, R. C. (2007). Functional specialisation of the thoracic limb of the hare (Lepus europeus). *Journal of Anatomy*, **210**(4), 491–505.

Yakovenko, S., & Drew, T. (2015). Similar Motor Cortical Control Mechanisms for Precise Limb Control during Reaching and Locomotion. *The Journal of Neuroscience*, **35**(43), 14476–14490.

Yakovenko, S., Mushahwar, V., VanderHorst, V., Holstege, G., & Prochazka, A. (2002). Spatiotemporal activation of lumbosacral motoneurons in the locomotor step cycle. *Journal of Neurophysiology*, **87**(3), 1542–1553.

Young, R. P., Scott, S. H., & Loeb, G. E. (1993). The distal hindlimb musculature of the cat: Multiaxis moment arms at the ankle joint. *Experimental Brain Research*, **96**(1), 141–151.

Additional information

Data availability statement

Raw morphological data are provided in supplemental material. Additional data will be made available on request. MATLAB code for computing all variables presented in the article is available at https://github.com/BorisPrilutskyLab/CatForelimbNeuromechanics.

Competing interests

The authors have no conflicts of interest.

Author contributions

B.I.P., T.J.B., A.F. and I.A.R. conceived and designed research. R.S.M., N.E.B., T.R.N. and T.J.B. performed forelimb dissections and morphological measurements and modelling. A.N.K. and B.I.P. recorded mechanics of locomotion. A.F. provided EMG recordings. S.M.R. developed the 2D forelimb model and computed motor and sensory signals during locomotion. S.M.R. and J.A.M. performed sensitivity analysis of the model. S.M.R. and B.I.P. prepared figures. S.M.R., R.S.M., N.E.B, T.J.B. and B.I.P. drafted manuscript. All authors discussed, reviewed and edited the final version of the manuscript. All authors have read and approved the final version of this manuscript and agree to be accountable for all aspects of the work in ensuring that questions related to the accuracy or integrity of any part of the work are appropriately investigated and resolved. All persons designated as authors qualify for authorship, and all those who qualify for authorship are listed.

Funding

This study was supported by US NIH grants HD032571 and R01 NS110550 and US NSF grant 2024414.

Keywords

cat, forelimb, locomotion, sensorimotor control

Supporting information

Additional supporting information can be found online in the Supporting Information section at the end of the HTML view of the article. Supporting information files available:

Peer Review History
Supplement 1
Supplement 2
Supplement 3
Supplement 4